FastGRNN: A Fast, Accurate, Stable and Tiny Kilobyte Sized Gated Recurrent Neural Network

Aditya Kusupati[†], **Manish Singh**[§], **Kush Bhatia**[‡],
Ashish Kumar[‡], **Prateek Jain**[†] **and Manik Varma**[†]
[†]Microsoft Research India
[§]Indian Institute of Technology Delhi
[‡]University of California Berkeley
{t-vekusu,prajain,manik}@microsoft.com, singhmanishiitd@gmail.com
kush@cs.berkeley.edu, ashish_kumar@berkeley.edu

Abstract

This paper develops the FastRNN and FastGRNN algorithms to address the twin RNN limitations of inaccurate training and inefficient prediction. Previous approaches have improved accuracy at the expense of prediction costs making them infeasible for resource-constrained and real-time applications. Unitary RNNs have increased accuracy somewhat by restricting the range of the state transition matrix's singular values but have also increased the model size as they require a larger number of hidden units to make up for the loss in expressive power. Gated RNNs have obtained state-of-the-art accuracies by adding extra parameters thereby resulting in even larger models. FastRNN addresses these limitations by adding a residual connection that does not constrain the range of the singular values explicitly and has only two extra scalar parameters. FastGRNN then extends the residual connection to a gate by reusing the RNN matrices to match state-of-the-art gated RNN accuracies but with a 2-4x smaller model. Enforcing FastGRNN's matrices to be low-rank, sparse and quantized resulted in accurate models that could be up to 35x smaller than leading gated and unitary RNNs. This allowed FastGRNN to accurately recognize the "Hey Cortana" wakeword with a 1 KB model and to be deployed on severely resource-constrained IoT microcontrollers too tiny to store other RNN models. FastGRNN's code is available at [30].

1 Introduction

Objective: This paper develops the FastGRNN (an acronym for a Fast, Accurate, Stable and Tiny Gated Recurrent Neural Network) algorithm to address the twin RNN limitations of inaccurate training and inefficient prediction. FastGRNN almost matches the accuracies and training times of state-of-the-art unitary and gated RNNs but has significantly lower prediction costs with models ranging from 1 to 6 Kilobytes for real-world applications.

RNN training and prediction: It is well recognized that RNN training is inaccurate and unstable as non-unitary hidden state transition matrices could lead to exploding and vanishing gradients for long input sequences and time series. An equally important concern for resource-constrained and real-time applications is the RNN's model size and prediction time. Squeezing the RNN model and code into a few Kilobytes could allow RNNs to be deployed on billions of Internet of Things (IoT) endpoints having just 2 KB RAM and 32 KB flash memory [17, 29]. Similarly, squeezing the RNN model and code into a few Kilobytes of the 32 KB L1 cache of a Raspberry Pi or smartphone, could significantly reduce the prediction time and energy consumption and make RNNs feasible for real-

32nd Conference on Neural Information Processing Systems (NeurIPS 2018), Montréal, Canada.

time applications such as wake word detection [27, 11, 12, 42, 43], predictive maintenance [46, 1], human activity recognition [3, 2], *etc*.

Unitary and gated RNNs: A number of techniques have been proposed to stabilize RNN training based on improved optimization algorithms [40, 26], unitary RNNs [5, 24, 37, 47, 50, 54, 25] and gated RNNs [20, 13, 14]. While such approaches have increased the RNN prediction accuracy they have also significantly increased the model size. Unitary RNNs have avoided gradients exploding and vanishing by limiting the range of the singular values of the hidden state transition matrix. This has led to only limited gains in prediction accuracy as the optimal transition matrix might often not be close to unitary. Unitary RNNs have compensated by learning higher dimensional representations but, unfortunately, this has led to larger model sizes. Gated RNNs [20, 13, 14] have stabilized training by adding extra parameters leading to state-of-the-art prediction accuracies but with models that might sometimes be even larger than unitary RNNs.

FastRNN: This paper demonstrates that standard RNN training could be stabilized with the addition of a residual connection [19, 44, 22, 7] having just 2 additional scalar parameters. Residual connections for RNNs have been proposed in [22] and further studied in [7]. This paper proposes the FastRNN architecture and establishes that a simple variant of [22, 7] with learnt weighted residual connections (2) can lead to provably stable training and near state-of-the-art prediction accuracies with lower prediction costs than all unitary and gated RNNs. In particular, FastRNN's prediction accuracies could be: (a) up to 19% higher than a standard RNN; (b) could often surpass the accuracies of all unitary RNNs and (c) could be just shy of the accuracies of leading gated RNNs. FastRNN's empirical performance could be understood on the basis of theorems proving that for an input sequence with T steps and appropriate setting of residual connection weights: (a) FastRNN converges to a stationary point within $O(1/\epsilon^2)$ SGD iterations, independent of T, while the *same analysis* for a standard RNN reveals an upper bound of $O(2^T)$ iterations and (b) FastRNN's generalization error bound is independent of T whereas the *same proof technique* reveals an exponential bound for standard RNNs.

FastGRNN: Inspired by this analysis, this paper develops the novel FastGRNN architecture by converting the residual connection to a gate while reusing the RNN matrices. This allowed FastGRNN to match, and sometimes exceed, state-of-the-art prediction accuracies of LSTMs, GRUs, UGRNNs and other leading gated RNN techniques while having 2-4x fewer parameters. Enforcing FastGRNN's matrices to be low-rank, sparse and quantized led to a minor decrease in the prediction accuracy but resulted in models that could be up to 35x smaller and fit in 1-6 Kilobytes for many applications. For instance, using a 1 KB model, FastGRNN could match the prediction accuracies of all other RNNs at the task of recognizing the "Hey Cortana" wakeword. This allowed FastGRNN to be deployed on IoT endpoints, such as the Arduino Uno, which were too small to hold other RNN models. On slightly larger endpoints, such as the Arduino MKR1000 or Due, FastGRNN was found to be 18-42x faster at making predictions than other leading RNN methods.

Contributions: This paper makes two contributions. First, it rigorously studies the residual connection based FastRNN architecture which could often outperform unitary RNNs in terms of training time, prediction accuracy and prediction cost. Second, inspired by FastRNN, it develops the FastGRNN architecture which could almost match state-of-the-art accuracies and training times but with prediction costs that could be lower by an order of magnitude. FastRNN and FastGRNN's code can be downloaded from [30].

2 Related Work

Residual connections: Residual connections have been studied extensively in CNNs [19, 44] as well as RNNs [22, 7]. The Leaky Integration Unit architecture [22] proposed residual connections for RNNs but were unable to learn the state transition matrix due to the problem of exploding and vanishing gradients. They therefore sampled the state transition matrix from a hand-crafted distribution with spectral radius less than one. This limitation was addressed in [7] where the state transition matrix was learnt but the residual connections were applied to only a few hidden units and with randomly sampled weights. Unfortunately, the distribution from which the weights were sampled could lead to an ill-conditioned optimization problem. In contrast, the FastRNN architecture leads to provably stable training with just two learnt weights connected to all the hidden units.

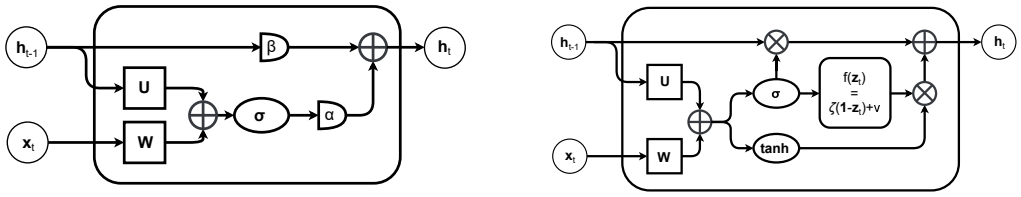

(a) FastRNN - Residual Connection

(b) FastGRNN - Gate

Figure 1: Block diagrams for FastRNN (a) and FastGRNN (b). FastGRNN uses shared matrices $\mathbf{W}$, $\mathbf{U}$ to compute both the hidden state $\mathbf{h}_t$ as well as the gate $\mathbf{z}_t$.

Unitary RNNs: Unitary RNNs [5, 50, 37, 24, 47, 25] stabilize RNN training by learning only well-conditioned state transition matrices. This limits their expressive power and prediction accuracy while increasing training time. For instance, SpectralRNN [54] learns a transition matrix with singular values in $1 \pm \epsilon$. Unfortunately, the training algorithm converged only for small ϵ thereby limiting accuracy on most datasets. Increasing the number of hidden units was found to increase accuracy somewhat but at the cost of increased training time, prediction time and model size.

Gated RNNs: Gated architectures [20, 13, 14, 23] achieve state-of-the-art classification accuracies by adding extra parameters but also increase model size and prediction time. This has resulted in a trend to reduce the number of gates and parameters with UGRNNs [14] simplifying GRUs [13] which in turn simplify LSTMs [20]. FastGRNN can be seen as a natural simplification of UGRNN where the RNN matrices are reused within the gate and are made low-rank, sparse and quantized so as to compress the model.

Efficient training and prediction: Efficient prediction algorithms have often been obtained by making sparsity and low-rank assumptions. Most unitary methods effectively utilize a low-rank representation of the state transition matrix to control prediction and training complexity [24, 54]. Sparsity, low-rank, and quantization were shown to be effective in RNNs [51, 39, 48], CNNs [18], trees [29] and nearest neighbour classifiers [17]. FastGRNN builds on these ideas to utilize low-rank, sparse and quantized representations for learning kilobyte sized classifiers without compromising on classification accuracy. Other approaches to speed up RNN training and prediction are based on replacing sequential hidden state transitions by parallelizable convolutions [9] or on learning skip connections [10] so as to avoid evaluating all the hidden states. Such techniques are complementary to the ones proposed in this paper and can be used to further improve FastGRNN's performance.

3 FastRNN and FastGRNN

Notation: Throughout the paper, parameters of an RNN are denoted by matrices $\mathbf{W} \in \mathbb{R}^{\hat{D} \times D}$, $\mathbf{U} \in \mathbb{R}^{\hat{D} \times \hat{D}}$ and bias vectors $\mathbf{b} \in \mathbb{R}^{\hat{D}}$, often using subscripts if multiple vectors are required to specify the architecture. $\mathbf{a} \odot \mathbf{b}$ denotes the Hadamard product between $\mathbf{a}$ and $\mathbf{b}$, i.e., $(\mathbf{a} \odot \mathbf{b})_i = \mathbf{a}_i, \mathbf{b}_i$. $\|\cdot\|_0$ denotes the number of non-zeros entries in a matrix or vector. $\|\cdot\|_F$, $\|\cdot\|_2$ denotes the Frobenius and spectral norm of a matrix, respectively. Unless specified, $\|\cdot\|$ denotes $\|\cdot\|_2$ of a matrix or vector. $\mathbf{a}^\top \mathbf{b} = \sum_i a_i b_i$ denotes the inner product of $\mathbf{a}$ and $\mathbf{b}$.

Standard RNN architecture [41] is known to be *unstable* for training due to exploding or vanishing gradients and hence is shunned for more expensive gated architectures.

This paper studies the FastRNN architecture that is inspired by weighted residual connections [22, 19], and shows that FastRNN can be significantly more stable and accurate than the standard RNN while preserving its prediction complexity. In particular, Section 3.1.1 demonstrates parameter settings for FastRNN that guarantee well-conditioned gradients as well as faster convergence rate and smaller generalization error than the standard RNN. This paper further strengthens FastRNN to develop the FastGRNN architecture that is more accurate than unitary methods [5, 54] and provides comparable accuracy to the state-of-the-art gated RNNs at 35x less computational cost (see Table 3).

3.1 FastRNN

Let $\mathbf{X} = [\mathbf{x}_1, \ldots, \mathbf{x}_T]$ be the input data where $\mathbf{x}_t \in \mathbb{R}^D$ denotes the t-th step feature vector. Then, the goal of multi-class RNNs is to learn a function $F : \mathbb{R}^{D \times T} \to \{1, \ldots, L\}$ that predicts one of L classes for the given data point $\mathbf{X}$. Standard RNN architecture has a provision to produce an output at every time step, but we focus on the setting where each data point is associated with a single label that is predicted at the end of the time horizon T. Standard RNN maintains a vector of hidden state $\mathbf{h}_t \in \mathbb{R}^{\hat{D}}$ which captures temporal dynamics in the input data, i.e.,

$$\mathbf{h}_t = \tanh(\mathbf{W}\mathbf{x}_t + \mathbf{U}\mathbf{h}_{t-1} + \mathbf{b}). \tag{1}$$

As explained in the next section, learning $\mathbf{U}, \mathbf{W}$ in the above architecture is difficult as the gradient can have exponentially large (in T) condition number. Unitary methods explicitly control the condition number of the gradient but their training time can be significantly larger or the generated model can be less accurate.

Instead, FastRNN uses a simple weighted residual connection to stabilize the training by generating well-conditioned gradients. In particular, FastRNN updates the hidden state $\mathbf{h}_t$ as follows:

$$\begin{aligned} \tilde{\mathbf{h}}_t &= \sigma(\mathbf{W}\mathbf{x}_t + \mathbf{U}\mathbf{h}_{t-1} + \mathbf{b}), \\ \mathbf{h}_t &= \alpha\tilde{\mathbf{h}}_t + \beta\mathbf{h}_{t-1}, \end{aligned} \tag{2}$$

where $0 \leq \alpha, \beta \leq 1$ are trainable weights that are parameterized by the sigmoid function. $\sigma : \mathbb{R} \to \mathbb{R}$ is a non-linear function such as $\tanh$, sigmoid, or ReLU, and can vary across datasets. Given $\mathbf{h}_T$, the label for a given point $\mathbf{X}$ is predicted by applying a standard classifier, e.g., logistic regression to $\mathbf{h}_T$.

Typically, $\alpha \ll 1$ and $\beta \approx 1 - \alpha$, especially for problems with larger T. FastRNN updates hidden state in a controlled manner with α, β limiting the extent to which the current feature vector $\mathbf{x}_t$ updates the hidden state. Also, FastRNN has only 2 more parameters than RNN and require only $\hat{D}$ more computations, which is a tiny fraction of per-step computation complexity of RNN. Unlike unitary methods [5, 23, 54], FastRNN does not introduce expensive structural constraints on $\mathbf{U}$ and hence scales well to large datasets with standard optimization techniques [28].

3.1.1 Analysis

This section shows how FastRNN addresses the issue of ill-conditioned gradients, leading to stable training and smaller generalization error. For simplicity, assume that the label decision function is one dimensional and is given by $f(\mathbf{X}) = \mathbf{v}^\top \mathbf{h}_T$. Let $L(\mathbf{X}, y; \theta) = L(f(\mathbf{X}), y; \theta)$ be the logistic loss function for the given labeled data point $(\mathbf{X}, y)$ and with parameters $\theta = (\mathbf{W}, \mathbf{U}, \mathbf{v})$. Then, the gradient of L w.r.t. $\mathbf{W}, \mathbf{U}, \mathbf{v}$ is given by:

$$\frac{\partial L}{\partial \mathbf{U}} = \alpha \sum_{t=0}^{T} \mathbf{D}_t \left(\prod_{k=t}^{T-1} (\alpha \mathbf{U}^\top \mathbf{D}_{k+1} + \beta \mathbf{I}) \right) (\nabla_{\mathbf{h}_T} L) \mathbf{h}_{t-1}^\top, \tag{3}$$

$$\frac{\partial L}{\partial \mathbf{W}} = \alpha \sum_{t=0}^{T} \mathbf{D}_t \left(\prod_{k=t}^{T-1} (\alpha \mathbf{U}^\top \mathbf{D}_{k+1} + \beta \mathbf{I}) \right) (\nabla_{\mathbf{h}_T} L) \mathbf{x}_t^\top, \frac{\partial L}{\partial \mathbf{v}} = \frac{-y \exp\left(-y \cdot \mathbf{v}^\top \mathbf{h}_T\right)}{1 + \exp\left(-y \cdot \mathbf{v}^\top \mathbf{h}_T\right)} \mathbf{h}_T, \tag{4}$$

where $\nabla_{\mathbf{h}_T} L = -c(\theta) \cdot y \cdot \mathbf{v}$, and $c(\theta) = \frac{1}{1+\exp\left(y \cdot \mathbf{v}^\top \mathbf{h}_T\right)}$. A critical term in the above expression is: $M(\mathbf{U}) = \prod_{k=t}^{T-1} (\alpha \mathbf{U}^\top \mathbf{D}_{k+1} + \beta \mathbf{I})$, whose condition number, $\kappa_{M(\mathbf{U})}$, is bounded by:

$$\kappa_{M(\mathbf{U})} \leq \frac{(1 + \frac{\alpha}{\beta} \max_k \|\mathbf{U}^\top \mathbf{D}_{k+1}\|)^{T-t}}{(1 - \frac{\alpha}{\beta} \max_k \|\mathbf{U}^\top \mathbf{D}_{k+1}\|)^{T-t}}, \tag{5}$$

where $\mathbf{D}_k = \text{diag}(\sigma'(\mathbf{W}\mathbf{x}_k + \mathbf{U}\mathbf{h}_{k-1} + \mathbf{b}))$ is the Jacobian matrix of the pointwise nonlinearity. Also if $\alpha = 1$ and $\beta = 0$, which corresponds to standard RNN, the condition number of $M(\mathbf{U})$ can be as large as $(\max_k \frac{\|\mathbf{U}^\top \mathbf{D}_{k+1}\|}{\lambda_{min}(\mathbf{U}^\top \mathbf{D}_{k+1})})^{T-t}$ where $\lambda_{min}(\mathbf{A})$ denotes the minimum singular value of $\mathbf{A}$. Hence, gradient's condition number for the standard RNN can be exponential in T. This implies that, relative to the average eigenvalue, the gradient can explode or vanish in certain directions, leading to unstable training.

In contrast to the standard RNN, if $\beta \approx 1$ and $\alpha \approx 0$, then the condition number, $\kappa_{M(\mathbf{U})}$, for FastRNN is bounded by a small term. For example, if $\beta = 1 - \alpha$ and $\alpha = \frac{1}{T \max_k \|\mathbf{U}^\top \mathbf{D}_{k+1}\|}$,

then $\kappa_{M(\mathbf{U})} = O(1)$. Existing unitary methods are also motivated by similar observation. But they attempt to control the $\kappa_{M(\mathbf{U})}$ by restricting the condition number, $\kappa_{\mathbf{U}}$, of $\mathbf{U}$ which can still lead to ill-conditioned gradients as $\mathbf{U}^\top \mathbf{D}_{k+1}$ might still be very small in certain directions. By using residual connections, FastRNN is able to address this issue, and hence have faster training and more accurate model than the state-of-the-art unitary RNNs.

Finally, by using the above observations and a careful perturbation analysis, we can provide the following convergence and generalization error bounds for FastRNN:

Theorem 3.1 (Convergence Bound). *Let $[(\mathbf{X}_1, y_1), \ldots, (\mathbf{X}_n, y_n)]$ be the given labeled sequential training data. Let $L(\theta) = \frac{1}{n}\sum_i L(\mathbf{X}_i, y_i; \theta)$ be the loss function with $\theta = (\mathbf{W}, \mathbf{U}, \mathbf{v})$ be the parameters of FastRNN architecture (2) with $\beta = 1 - \alpha$ and α such that*

$$\alpha \leq \min\left(\frac{1}{4T \cdot |\mathcal{D}\|\mathbf{U}\|_2 - 1|}, \frac{1}{4T \cdot R_{\mathbf{U}}}, \frac{1}{T \cdot |\|\mathbf{U}\|_2 - 1|}\right),$$

where $\mathcal{D} = \sup_{\theta,k} \|\mathbf{D}_k^\theta\|_2$. Then, randomized stochastic gradient descent [15], a minor variation of SGD, when applied to the data for a maximum of M iteration outputs a solution $\widehat{\theta}$ such that:

$$\mathbb{E}[\|\nabla_\theta L(\widehat{\theta})\|_2^2\|] \leq \mathcal{B}_M := \frac{\mathcal{O}(\alpha T) L(\theta_0)}{M} + \left(\bar{D} + \frac{4R_{\mathbf{W}} R_{\mathbf{U}} R_{\mathbf{v}}}{\bar{D}}\right) \frac{\mathcal{O}(\alpha T)}{\sqrt{M}},$$

where $R_{\mathbf{X}} = \max_{\mathbf{X}} \|\mathbf{X}\|_F$ for $\mathbf{X} = \{\mathbf{U}, \mathbf{W}, \mathbf{v}\}$, $L(\theta_0)$ is the loss of the initial classifier, and the step-size of the k-th SGD iteration is fixed as: $\gamma_k = \min\left\{\frac{1}{\mathcal{O}(\alpha T)}, \frac{\bar{D}}{T\sqrt{M}}\right\}, k \in [M], \ \bar{D} \geq 0$.

Theorem 3.2 (Generalization Error Bound). *[6] Let $\mathcal{Y}, \hat{\mathcal{Y}} \subseteq [0, 1]$ and let $\mathcal{F}_T$ denote the class of FastRNN with $\|\mathbf{U}\|_F \leq R_{\mathbf{U}}, \|\mathbf{W}\|_F \leq R_{\mathbf{W}}$. Let the final classifier be given by $\sigma(\mathbf{v}^\top \mathbf{h}_T)$, $\|\mathbf{v}\|_2 \leq R_{\mathbf{v}}$. Let $L : \mathcal{Y} \times \hat{\mathcal{Y}} \to [0, B]$ be any 1-Lipschitz loss function. Let D be any distribution on $\mathcal{X} \times \mathcal{Y}$ such that $\|\mathbf{x}_{it}\|_2 \leq R_x$ a.s. Let $0 \leq \delta \leq 1$. For all $\beta = 1 - \alpha$ and alpha such that,*

$$\alpha \leq \min\left(\frac{1}{4T \cdot |\mathcal{D}\|\mathbf{U}\|_2 - 1|}, \frac{1}{4T \cdot R_{\mathbf{U}}}, \frac{1}{T \cdot |\|\mathbf{U}\|_2 - 1|}\right).$$

where $\mathcal{D} = \sup_{\theta,k} \|\mathbf{D}_k^\theta\|_2$, we have that with probability at least $1 - \delta$, all functions $f \in \mathbf{v} \circ \mathcal{F}_T$ satisfy,

$$\mathbb{E}_D[L(f(\mathbf{X}), y)] \leq \frac{1}{n}\sum_{i=1}^{n} L(f(\mathbf{X}_i), y_i) + \mathcal{C}\frac{O(\alpha T)}{\sqrt{n}} + B\sqrt{\frac{\ln(\frac{1}{\delta})}{n}},$$

where $\mathcal{C} = R_{\mathbf{W}} R_{\mathbf{U}} R_{\mathbf{x}} R_{\mathbf{v}}$ represents the boundedness of the parameter matrices and the data.

The convergence bound states that if $\alpha = O(1/T)$ then the algorithm converges to a stationary point in polynomial time (in M), while generalization bound states that for $\alpha = O(1/T)$, the generalization error of FastRNN is *independent* of T. In contrast, *similar proof technique* provide exponentially poor (in T) error bound and convergence rate for standard RNN. But, this is an upper bound, so potentially significantly better error bounds for RNN might exist; matching lower bound results for standard RNN is an interesting research direction. Also, $O(T^2)$ generalization error bound can be argued using VC-dimension style arguments [4]. But such bounds hold for specific settings like binary y, and are independent of problem hardness parameterized by the size of the weight matrices $(R_{\mathbf{W}}, R_{\mathbf{U}})$.

Finally, note that the above analysis fixes $\alpha = O(1/T)$, $\beta = 1 - \alpha$, but in practice FastRNN learns α, β (which is similar to performing cross-validation on α, β). However, interestingly, across datasets the learnt α, β values indeed display a similar scaling wrt T for large T (see Figure 2).

3.2 FastGRNN

While FastRNN controls the condition number of gradient reasonably well, its expressive power might be limited for some datasets. This concern is addressed by a novel architecture, FastGRNN, that uses a scalar weighted residual connection for each and every coordinate of the hidden state $\mathbf{h}_t$. That is,

$$\begin{aligned}
\mathbf{z}_t &= \sigma(\mathbf{W}\mathbf{x}_t + \mathbf{U}\mathbf{h}_{t-1} + \mathbf{b}_z), \\
\tilde{\mathbf{h}}_t &= \tanh(\mathbf{W}\mathbf{x}_t + \mathbf{U}\mathbf{h}_{t-1} + \mathbf{b}_h), \\
\mathbf{h}_t &= (\zeta(\mathbf{1} - \mathbf{z}_t) + \nu) \odot \tilde{\mathbf{h}}_t + \mathbf{z}_t \odot \mathbf{h}_{t-1},
\end{aligned} \tag{6}$$

where $0 \leq \zeta, \nu \leq 1$ are trainable parameters that are parameterized by the sigmoid function, and $\sigma : \mathbb{R} \rightarrow \mathbb{R}$ is a non-linear function such as $\tanh$, sigmoid and can vary across datasets. Note that each coordinate of $\mathbf{z}_t$ is similar to parameter β in (2) and $\zeta(\mathbf{1} - \mathbf{z}_t) + \nu$'s coordinates simulate α parameter; also if $\nu \approx 0, \zeta \approx 1$ then it satisfies the intuition that $\alpha + \beta = 1$. It was observed that across all datasets, this gating mechanism outperformed the simple vector extension of FastRNN where each coordinate of α and β is learnt (see Appendix G).

FastGRNN computes each coordinate of gate $\mathbf{z}_t$ using a non-linear function of $\mathbf{x}_t$ and $\mathbf{h}_{t-1}$. To minimize the number of parameters, FastGRNN reuses the matrices $\mathbf{W}$, $\mathbf{U}$ for the vector-valued gating function as well. Hence, FastGRNN's inference complexity is almost same as that of the standard RNN but its accuracy and training stability is on par with expensive gated architectures like GRUs and LSTMs.

Sparse low-rank representation: FastGRNN further compresses the model size by using a low-rank and a sparse representation of the parameter matrices $\mathbf{W}$, $\mathbf{U}$. That is,

$$\mathbf{W} = \mathbf{W}^1(\mathbf{W}^2)^\top, \ \mathbf{U} = \mathbf{U}^1(\mathbf{U}^2)^\top, \ \|\mathbf{W}^i\|_0 \leq s_w^i, \ \|\mathbf{U}^i\|_0 \leq s_u^i, \ i = \{1, 2\}, \tag{7}$$

where $\mathbf{W}^1 \in \mathbb{R}^{\hat{D} \times r_w}, \mathbf{W}^2 \in \mathbb{R}^{D \times r_w}$, and $\mathbf{U}^1, \mathbf{U}^2 \in \mathbb{R}^{\hat{D} \times r_u}$. Hyperparameters r_w, s_w, r_u, s_u provide an efficient way to control the *accuracy-memory* trade-off for FastGRNN and are typically set via fine-grained validation. In particular, such compression is critical for FastGRNN model to fit on resource-constrained devices. Second, this low-rank representation brings down the prediction time by reducing the cost at each time step from $\mathcal{O}(\hat{D}(D + \hat{D}))$ to $\mathcal{O}(r_w(D + \hat{D}) + r_u\hat{D})$. This enables FastGRNN to provide on-device prediction in real-time on battery constrained devices.

3.2.1 Training FastGRNN

The parameters for FastGRNN: $\mathbf{\Theta}_{\text{FastGRNN}} = (\mathbf{W}^i, \mathbf{U}^i, \mathbf{b}_h, \mathbf{b}_z, \zeta, \nu)$ are trained jointly using projected batch stochastic gradient descent (b-SGD) (or other stochastic optimization methods) with typical batch sizes ranging from $64 - 128$. In particular, the optimization problem is given by:

$$\min_{\Theta_{\text{FastGRNN}}, \|\mathbf{W}^i\|_0 \leq s_w^i, \|\mathbf{U}^i\|_0 \leq s_u^i, i \in \{1,2\}} \mathcal{J}(\Theta_{\text{FastGRNN}}) = \frac{1}{n} \sum_j L(\mathbf{X}_j, y_j; \Theta_{\text{FastGRNN}}) \tag{8}$$

where L denotes the appropriate loss function (typically softmax cross-entropy). The training procedure for FastGRNN is divided into 3 stages:

(I) Learning low-rank representation (L): In the first stage of the training, FastGRNN is trained for e_1 epochs with the model as specified by (7) using b-SGD. This stage of optimization ignores the sparsity constraints on the parameters and learns a low-rank representation of the parameters.

(II) Learning sparsity structure (S): FastGRNN is next trained for e_2 epochs using b-SGD, projecting the parameters onto the space of sparse low-rank matrices after every few batches while maintaining support between two consecutive projection steps. This stage, using b-SGD with Iterative Hard Thresholding (IHT), helps FastGRNN identify the correct support for parameters $(\mathbf{W}^i, \mathbf{U}^i)$.

(III) Optimizing with fixed parameter support: In the last stage, FastGRNN is trained for e_3 epochs with b-SGD while freezing the support set of the parameters.

In practice, it is observed that $e_1 = e_2 = e_3 = 100$ generally leads to the convergence of FastGRNN to a good solution. Early stopping is often deployed in stages (II) and (III) to obtain the best models.

3.3 Byte Quantization (Q)

FastGRNN further compresses the model by quantizing each element of $\mathbf{W}^i, \mathbf{U}^i$, restricting them to at most one byte along with byte indexing for sparse models. However, simple integer quantization of $\mathbf{W}^i, \mathbf{U}^i$ leads to a large loss in accuracy due to gross approximation. Moreover, while such a quantization reduces the model size, the prediction time can still be large as non-linearities will require all the hidden states to be floating point. FastGRNN overcomes these shortcomings by training $\mathbf{W}^i$ and $\mathbf{U}^i$ using *piecewise-linear* approximation of the non-linear functions, thereby ensuring that all the computations can be performed with integer arithmetic. During training, FastGRNN replaces the non-linear function in (6) with their respective approximations and uses the above mentioned training procedure to obtain $\mathbf{\Theta}_{\text{FastGRNN}}$. The floating point parameters are then jointly quantized to ensure that all the relevant entities are integer-valued and the entire inference computation can

be executed efficiently with integer arithmetic without a significant drop in accuracy. For instance, Tables 4, 5 show that on several datasets FastGRNN models are 3-4x faster than their corresponding FastGRNN-Q models on common IoT boards with no floating point unit (FPU). FastGRNN-LSQ, FastGRNN "minus" the Low-rank, Sparse and Quantized components, is the base model with no compression.

4 Experiments

Datasets: FastRNN and FastGRNN's performance was benchmarked on the following IoT tasks where having low model sizes and prediction times was critical to the success of the application: (a) Wakeword-2 [45] - detecting utterances of the "Hey Cortana" wakeword; (b) Google-30 [49] and Google-12 - detection of utterances of 30 and 10 commands plus background noise and silence and (c) HAR-2 [3] and DSA-19 [2] - Human Activity Recognition (HAR) from an accelerometer and gyroscope on a Samsung Galaxy S3 smartphone and Daily and Sports Activity (DSA) detection from a resource-constrained IoT wearable device with 5 Xsens MTx sensors having accelerometers, gyroscopes and magnetometers on the torso and four limbs. Traditional RNN tasks typically do not have prediction constraints and are therefore not the focus of this paper. Nevertheless, for the sake of completeness, experiments were also carried out on benchmark RNN tasks such as language modeling on the Penn Treebank (PTB) dataset [33], star rating prediction on a scale of 1 to 5 of Yelp reviews [52] and classification of MNIST images on a pixel-by-pixel sequence [32, 31].

All datasets, apart from Wakeword-2, are publicly available and their pre-processing and feature extraction details are provided in Appendix B. The publicly provided training set for each dataset was subdivided into 80% for training and 20% for validation. Once the hyperparameters had been fixed, the algorithms were trained on the full training set and results were reported on the publicly available test set. Table 1 lists the statistics of all datasets.

Baseline algorithms and Implementation: FastRNN and FastGRNN were compared to standard RNNs [41], leading unitary RNN approaches such as SpectralRNNs [54], Orthogonal RNNs (oRNN) [37], Efficient Unitary Recurrent Neural Networks (EURNN) [24], FactoredRNNs [47] and state-of-the-art gated RNNs including UGRNNs [14], GRUs [13] and LSTMs [20]. Details of these methods are provided in Section 2. Native Tensorflow implementations were used for the LSTM and GRU architectures. For all the other RNNs, publicly available implementations provided by the authors were used taking care to ensure that published results could be reproduced thereby verifying the code and hyper-parameter settings. All experiments were run on an Nvidia Tesla P40 GPU with CUDA 9.0 and cuDNN 7.1 on a machine with an Intel Xeon 2.60 GHz CPU with 12 cores.

Hyper-parameters: The hyper-parameters of each algorithm were set by a fine-grained validation wherever possible or according to the settings recommended by the authors otherwise. Adam, Nesterov Momentum and SGD were used to optimize each algorithm on each dataset and the optimizer with the best validation performance was selected. The learning rate was initialized to 10^{-2} for all architectures except for RNNs where the learning rate was initialized to 10^{-3} to ensure stable training. Each algorithm was run for 200 epochs after which the learning rate was decreased by a factor of 10^{-1} and the algorithm run again for another 100 epochs. This procedure was carried out on all datasets except for Pixel MNIST where the learning rate was decayed by $\frac{1}{2}$ after each pass of 200 epochs. Batch sizes between 64 and 128 training points were tried for most architectures and a batch size of 100 was found to work well in general except for standard RNNs which required a batch size of 512. FastRNN used $\tanh$ as the non-linearity in most cases except for a few (indicated by $^+$) where ReLU gave slightly better results. Table 11 in the Appendix lists the non-linearity, optimizer and hyper-parameter settings for FastGRNN on all datasets.

Table 1: Dataset Statistics

Dataset	#Train	#Features	#Time Steps	#Test
Google-12	22,246	3,168	99	3,081
Google-30	51,088	3,168	99	6,835
Wakeword-2	195,800	5,184	162	83,915
Yelp-5	500,000	38,400	300	500,000
HAR-2	7,352	1,152	128	2,947
Pixel-MNIST-10	60,000	784	784	10,000
PTB-10000	929,589	—	300	82,430
DSA-19	4,560	5,625	125	4,560

Table 2: PTB Language Modeling - 1 Layer

Method	Test Perplexity	Train Perplexity	Model Size (KB)	Train Time (min)
RNN	144.71	68.11	129	**9.11**
FastRNN	127.76$^+$	109.07	513	11.20
FastGRNN-LSQ	**115.92**	89.58	513	12.53
FastGRNN	116.11	81.31	**39**	13.75
SpectralRNN	130.20	65.42	242	—
UGRNN	119.71	65.25	256	11.12
LSTM	117.41	69.44	2052	13.52

Evaluation criteria: The emphasis in this paper is on designing RNN architectures which can run on low-memory IoT devices and which are efficient at prediction time. As such, the model size of each architecture is reported along with its training time and classification accuracy (F1 score on the Wakeword-2 dataset and perplexity on the PTB dataset). Prediction times on some of the popular IoT boards are also reported. Note that, for NLP applications such as PTB and Yelp, just the model size of the various RNN architectures has been reported. In a real application, the size of the learnt word-vector embeddings (10 MB for FastRNN and FastGRNN) would also have to be considered.

Results: Tables 2 and 3 compare the performance of FastRNN, FastGRNN and FastGRNN-LSQ to state-of-the-art RNNs. Three points are worth noting about FastRNN's performance. First, FastRNN's prediction accuracy gains over a standard RNN ranged from 2.34% on the Pixel-MNIST dataset to 19% on the Google-12 dataset. Second, FastRNN's prediction accuracy could surpass leading unitary RNNs on 6 out of the 8 datasets with gains up to 2.87% and 3.77% over SpectralRNN on the Google-12 and DSA-19 datasets respectively. Third, FastRNN's training speedups over all unitary and gated RNNs could range from 1.2x over UGRNN on the Yelp-5 and DSA-19 datasets to 196x over EURNN on the Google-12 dataset. This demonstrates that the vanishing and exploding gradient problem could be overcome by the addition of a simple weighted residual connection to the standard RNN architecture thereby allowing FastRNN to train efficiently and stablely. This also demonstrates that the residual connection offers a theoretically principled architecture that can often result in accuracy gains without limiting the expressive power of the hidden state transition matrix.

Tables 2 and 3 also demonstrate that FastGRNN-LSQ could be more accurate and faster to train than all unitary RNNs. Furthermore, FastGRNN-LSQ could match the accuracies and training times of state-of-the-art gated RNNs while having models that could be 1.18-4.87x smaller. This demonstrates that extending the residual connection to a gate which reuses the RNN matrices increased accuracy with virtually no increase in model size over FastRNN in most cases. In fact, on Google-30 and Pixel-MNIST FastGRNN-LSQ's model size was lower than FastRNN's as it had a lower hidden dimension indicating that the gate efficiently increased expressive power.

Finally, Tables 2 and 3 show that FastGRNN's accuracy was at most 1.13% worse than the best RNN but its model could be up to 35x smaller even as compared to low-rank unitary methods such as SpectralRNN. Figures 3 and 4 in the Appendix also show that FastGRNN-LSQ and FastGRNN's classification accuracies could be higher than those obtained by the best unitary and gated RNNs for any given model size in the 0-128 KB range. This demonstrates the effectiveness of making FastGRNN's parameters low-rank, sparse and quantized and allows FastGRNN to fit on the Arduino

Table 3: FastGRNN had up to 35x smaller models than leading RNNs with almost no loss in accuracy

	Dataset	Google-12			Google-30			Wakeword-2		
	Method	Accuracy (%)	Model Size (KB)	Train Time (hr)	Accuracy (%)	Model Size (KB)	Train Time (hr)	F1 Score	Model Size (KB)	Train Time(hr)
	RNN	73.25	56	1.11	80.05	63	2.13	89.17	8	**0.28**
Proposed	FastRNN	92.21$^+$	56	**0.61**	91.60$^+$	96	**1.30**	97.09	8	0.69
Proposed	FastGRNN-LSQ	**93.18**	57	0.63	**92.03**	45	1.41	**98.19**	8	0.83
Proposed	FastGRNN	92.10	**5.5**	0.75	90.78	**6.25**	1.77	97.83	**1**	1.08
Unitary	SpectralRNN	91.59	228	19.00	88.73	128	11.00	96.75	17	7.00
Unitary	EURNN	76.79	210	120.00	56.35	135	19.00	92.22	24	69.00
Unitary	oRNN	88.18	102	16.00	86.95	120	35.00	—	—	—
Unitary	FactoredRNN	53.33	1114	7.00	40.57	1150	8.52	—	—	—
Gated	UGRNN	92.63	75	0.78	90.54	260	2.11	98.17	16	1.00
Gated	GRU	93.15	248	1.23	91.41	257	2.70	97.63	24	1.38
Gated	LSTM	92.30	212	1.36	90.31	219	2.63	97.82	32	1.71

	Dataset	Yelp-5			HAR-2			DSA-19			Pixel-MNIST-10		
	Method	Accuracy (%)	RNN Model Size (KB)	Train Time (hr)	Accuracy (%)	Model Size (KB)	Train Time (hr)	Accuracy (%)	Model Size (KB)	Train Time (min)	Accuracy (%)	Model Size (KB)	Train Time (hr)
	RNN	47.59	130	**3.33**	91.31	29	0.11	71.68	20	**1.11**	94.10	71	45.56
Proposed	FastRNN	55.38	130	3.61	94.50$^+$	29	**0.06**	84.14	97	1.92	96.44	166	15.10
Proposed	FastGRNN-LSQ	**59.51**	130	3.91	95.38	29	0.08	**85.00**	208	2.15	**98.72**	71	**12.57**
Proposed	FastGRNN	59.43	**8**	4.62	**95.59**	3	0.10	83.73	**3.25**	2.10	98.20	**6**	16.97
Unitary	SpectralRNN	56.56	89	4.92	95.48	525	0.73	80.37	50	2.25	97.70	25	—
Unitary	EURNN	59.01	122	72.00	93.11	12	0.84	—	—	—	95.38	64	122.00
Unitary	oRNN	—	—	—	94.57	22	2.72	72.52	18	—	97.20	49	—
Unitary	FactoredRNN	—	—	—	78.65	**1**	0.11	73.20	1154	—	94.60	125	—
Gated	UGRNN	58.67	258	4.34	94.53	37	0.12	84.74	399	2.31	97.29	84	15.17
Gated	GRU	59.02	388	8.12	93.62	71	0.13	84.84	270	2.33	98.70	123	23.67
Gated	LSTM	59.49	516	8.61	93.65	74	0.18	84.84	526	2.58	97.80	265	26.57

Table 4: Prediction time in ms on the Arduino MKR1000

Method	Google-12	HAR-2	Wakeword-2
FastGRNN	537	162	175
FastGRNN-Q	2282	553	755
RNN	12028	2249	2232
UGRNN	22875	4207	6724
SpectralRNN	70902	—	10144

Table 5: Prediction time in ms on the Arduino Due

Method	Google-12	HAR-2	Wakeword-2
FastGRNN	242	62	77
FastGRNN-Q	779	172	238
RNN	3472	590	653
UGRNN	6693	1142	1823
SpectralRNN	17766	55558	2691

Uno having just 2 KB RAM and 32 KB flash memory. In particular, FastGRNN was able to recognize the "Hey Cortana" wakeword just as accurately as leading RNNs but with a 1 KB model.

Prediction on IoT boards: Unfortunately, most RNNs were too large to fit on an Arduino Uno apart from FastGRNN. On the slightly more powerful Arduino MKR1000 having an ARM Cortex M0+ microcontroller operating at 48 MHz with 32 KB RAM and 256 KB flash memory, Table 4 shows that FastGRNN could achieve the same prediction accuracy while being 25-45x faster at prediction than UGRNN and 57-132x faster than SpectralRNN. Results on the even more powerful Arduino Due are presented in Table 5 while results on the Raspberry Pi are presented in Table 12 of the Appendix.

Ablations, extensions and parameter settings: Enforcing that FastGRNN's matrices be low-rank led to a slight increase in prediction accuracy and reduction in prediction costs as shown in the ablation experiments in Tables 8, 9 and 10 in the Appendix. Adding sparsity and quantization led to a slight drop in accuracy but resulted in significantly smaller models. Next, Table 16 in the Appendix shows that regularization and layering techniques [36] that have been proposed to increase the prediction accuracy of other gated RNNs are also effective for FastGRNN and can lead to reductions in perplexity on the PTB dataset. Finally, Figure 2 and Table 7 of the Appendix measure the agreement between FastRNN's theoretical analysis and empirical observations. Figure 2 (a) shows that the α learnt on datasets with T time steps is decreasing function of T and Figure 2 (b) shows that the learnt α and β follow the relation $\alpha/\beta \approx O(1/T)$ for large T which is one of the settings in which FastRNN's gradients stabilize and training converges quickly as proved by Theorems 3.1 and 3.2. Furthermore, β can be seen to be close to $1-\alpha$ for large T in Figure 2 (c) as assumed in Section 3.1.1 for the convergence of long sequences. For instance, the relative error between β and $1-\alpha$ for Google-12 with 99 timesteps was 2.15%, for HAR-2 with 128 timesteps was 3.21% and for MNIST-10 with 112 timesteps was 0.68%. However, for short sequences where there was a lower likelihood of gradients exploding or vanishing, β was found to deviate significantly from $1-\alpha$ as this led to improved prediction accuracy. Enforcing that $\beta = 1-\alpha$ on short sequences was found to drop accuracy by up to 1.5%.

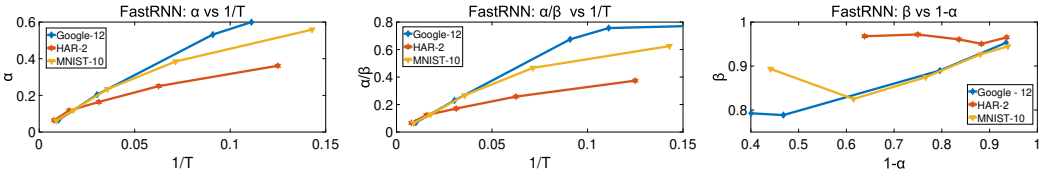

(a) (b) (c)

Figure 2: Plots (a) and (b) show the variation of α and α/β of FastRNN with respect to $1/T$ for three datasets. Plot (c) shows the relation between β and $1-\alpha$. In accordance with Theorem 3.1, the learnt values of α and α/β scale as $O(1/T)$ while $\beta \to 1-\alpha$ for long sequences.

5 Conclusions

This paper proposed the FastRNN and FastGRNN architectures for efficient RNN training and prediction. FastRNN could lead to provably stable training by incorporating a residual connection with two scalar parameters into the standard RNN architecture. FastRNN was demonstrated to have lower training times, lower prediction costs and higher prediction accuracies than leading unitary RNNs in most cases. FastGRNN extended the residual connection to a gate reusing the RNN matrices and was able to match the accuracies of state-of-the-art gated RNNs but with significantly lower prediction costs. FastGRNN's model could be compressed to 1-6 KB without compromising accuracy in many cases by enforcing that its parameters be low-rank, sparse and quantized. This allowed FastGRNN to make accurate predictions efficiently on severely resource-constrained IoT devices too tiny to hold other RNN models.

Acknowledgements

We are grateful to Ankit Anand, Niladri Chatterji, Kunal Dahiya, Don Dennis, Inderjit S. Dhillon, Dinesh Khandelwal, Shishir Patil, Adithya Pratapa, Harsha Vardhan Simhadri and Raghav Somani for helpful discussions and feedback. KB acknowledges the support of the NSF through grant IIS-1619362 and of the AFOSR through grant FA9550-17-1-0308.

References

[1] S. Ahmad, A. Lavin, S. Purdy, and Z. Agha. Unsupervised real-time anomaly detection for streaming data. *Neurocomputing*, 262:134–147, 2017.

[2] K. Altun, B. Barshan, and O. Tunçel. Comparative study on classifying human activities with miniature inertial and magnetic sensors. *Pattern Recognition*, 43(10):3605–3620, 2010. URL https://archive.ics.uci.edu/ml/datasets/Daily+and+Sports+Activities.

[3] D. Anguita, A. Ghio, L. Oneto, X. Parra, and J. L. Reyes-Ortiz. Human activity recognition on smartphones using a multiclass hardware-friendly support vector machine. In *International Workshop on Ambient Assisted Living*, pages 216–223. Springer, 2012. URL https://archive.ics.uci.edu/ml/datasets/human+activity+recognition+using+smartphones.

[4] M. Anthony and P. L. Bartlett. *Neural network learning: Theoretical foundations*. Cambridge University Press, 2009.

[5] M. Arjovsky, A. Shah, and Y. Bengio. Unitary evolution recurrent neural networks. In *International Conference on Machine Learning*, pages 1120–1128, 2016.

[6] P. L. Bartlett and S. Mendelson. Rademacher and gaussian complexities: Risk bounds and structural results. *Journal of Machine Learning Research*, 3(Nov):463–482, 2002.

[7] Y. Bengio, N. Boulanger-Lewandowski, and R. Pascanu. Advances in optimizing recurrent networks. In *Acoustics, Speech and Signal Processing (ICASSP), 2013 IEEE International Conference on*, pages 8624–8628. IEEE, 2013.

[8] K. Bhatia, K. Dahiya, H. Jain, Y. Prabhu, and M. Varma. The Extreme Classification Repository: Multi-label Datasets & Code. URL http://manikvarma.org/downloads/XC/XMLRepository.html.

[9] J. Bradbury, S. Merity, C. Xiong, and R. Socher. Quasi-recurrent neural networks. *arXiv preprint arXiv:1611.01576*, 2016.

[10] V. Campos, B. Jou, X. G. i Nieto, J. Torres, and S.-F. Chang. Skip RNN: Learning to skip state updates in recurrent neural networks. In *International Conference on Learning Representations*, 2018.

[11] G. Chen, C. Parada, and G. Heigold. Small-footprint keyword spotting using deep neural networks. In *Acoustics, Speech and Signal Processing (ICASSP), 2015 IEEE International Conference on*, pages 4087–4091. IEEE, 2014.

[12] G. Chen, C. Parada, and T. N. Sainath. Query-by-example keyword spotting using long short-term memory networks. In *Acoustics, Speech and Signal Processing (ICASSP), 2015 IEEE International Conference on*, pages 5236–5240. IEEE, 2015.

[13] K. Cho, B. Van Merriënboer, D. Bahdanau, and Y. Bengio. On the properties of neural machine translation: Encoder-decoder approaches. *arXiv preprint arXiv:1409.1259*, 2014.

[14] J. Collins, J. Sohl-Dickstein, and D. Sussillo. Capacity and trainability in recurrent neural networks. *arXiv preprint arXiv:1611.09913*, 2016.

[15] S. Ghadimi and G. Lan. Stochastic first-and zeroth-order methods for nonconvex stochastic programming. *SIAM Journal on Optimization*, 23(4):2341–2368, 2013.

[16] N. Golowich, A. Rakhlin, and O. Shamir. Size-independent sample complexity of neural networks. *arXiv preprint arXiv:1712.06541*, 2017.

[17] C. Gupta, A. S. Suggala, A. Gupta, H. V. Simhadri, B. Paranjape, A. Kumar, S. Goyal, M. Udupa, R. amd Varma, and P. Jain. Protonn: Compressed and accurate knn for resource-scarce devices. In *Proceedings of the International Conference on Machine Learning*, August 2017.

[18] S. Han, H. Mao, and W. J. Dally. Deep compression: Compressing deep neural networks with pruning, trained quantization and huffman coding. In *ICLR*, 2016.

[19] K. He, X. Zhang, S. Ren, and J. Sun. Deep residual learning for image recognition. In *Proceedings of the IEEE Conference on Computer Vision and Pattern Recognition*, pages 770–778, 2016.

[20] S. Hochreiter and J. Schmidhuber. Long short-term memory. *Neural computation*, 9(8): 1735–1780, 1997.

[21] H. Inan, K. Khosravi, and R. Socher. Tying word vectors and word classifiers: A loss framework for language modeling. *arXiv preprint arXiv:1611.01462*, 2016.

[22] H. Jaeger, M. Lukosevicius, D. Popovici, and U. Siewert. Optimization and applications of echo state networks with leaky-integrator neurons. *Neural Networks*, 20(3):335–352, 2007.

[23] L. Jing, C. Gulcehre, J. Peurifoy, Y. Shen, M. Tegmark, M. Soljacić, and Y. Bengio. Gated orthogonal recurrent units: On learning to forget. *arXiv preprint arXiv:1706.02761*, 2017.

[24] L. Jing, Y. Shen, T. Dubcek, J. Peurifoy, S. Skirlo, M. Tegmark, and M. Soljacić. Tunable efficient unitary neural networks (eunn) and their application to RNN. In *International Conference on Machine Learning*, 2017.

[25] C. Jose, M. Cisse, and F. Fleuret. Kronecker recurrent units. In J. Dy and A. Krause, editors, *International Conference on Machine Learning*, volume 80 of *Proceedings of Machine Learning Research*, pages 2380–2389, Stockholmsmässan, Stockholm Sweden, 10–15 Jul 2018. PMLR.

[26] S. Kanai, Y. Fujiwara, and S. Iwamura. Preventing gradient explosions in gated recurrent units. In *Advances in Neural Information Processing Systems*, pages 435–444, 2017.

[27] V. Këpuska and T. Klein. A novel wake-up-word speech recognition system, wake-up-word recognition task, technology and evaluation. *Nonlinear Analysis: Theory, Methods & Applications*, 71(12):e2772–e2789, 2009.

[28] D. P. Kingma and J. Ba. Adam: A method for stochastic optimization. *arXiv preprint arXiv:1412.6980*, 2014.

[29] A. Kumar, S. Goyal, and M. Varma. Resource-efficient machine learning in 2 kb ram for the internet of things. In *Proceedings of the International Conference on Machine Learning*, August 2017.

[30] A. Kusupati, M. Singh, K. Bhatia, A. Kumar, P. Jain, and M. Varma. The EdgeML Library: Code for FastRNN and FastGRNN, 2018. URL https://github.com/Microsoft/EdgeML.

[31] Q. V. Le, N. Jaitly, and G. E. Hinton. A simple way to initialize recurrent networks of rectified linear units. *arXiv preprint arXiv:1504.00941*, 2015.

[32] Y. LeCun, L. Bottou, Y. Bengio, and P. Haffner. Gradient-based learning applied to document recognition. *Proceedings of the IEEE*, 86(11):2278–2324, 1998.

[33] M. P. Marcus, M. A. Marcinkiewicz, and B. Santorini. Building a large annotated corpus of english: The penn treebank. *Computational linguistics*, 19(2):313–330, 1993.

[34] J. McAuley and J. Leskovec. Hidden factors and hidden topics: understanding rating dimensions with review text. In *Proceedings of the 7th ACM conference on Recommender systems*, pages 165–172. ACM, 2013.

[35] G. Melis, C. Dyer, and P. Blunsom. On the state of the art of evaluation in neural language models. *arXiv preprint arXiv:1707.05589*, 2017.

[36] S. Merity, N. S. Keskar, and R. Socher. Regularizing and optimizing LSTM language models. *arXiv preprint arXiv:1708.02182*, 2017.

[37] Z. Mhammedi, A. Hellicar, A. Rahman, and J. Bailey. Efficient orthogonal parametrisation of recurrent neural networks using householder reflections. In *International Conference on Machine Learning*, 2017.

[38] T. Mikolov and G. Zweig. Context dependent recurrent neural network language model. *SLT*, 12(234-239):8, 2012.

[39] S. Narang, E. Elsen, G. Diamos, and S. Sengupta. Exploring sparsity in recurrent neural networks. *arXiv preprint arXiv:1704.05119*, 2017.

[40] R. Pascanu, T. Mikolov, and Y. Bengio. On the difficulty of training recurrent neural networks. In *International Conference on Machine Learning*, pages 1310–1318, 2013.

[41] D. E. Rumelhart, G. E. Hinton, and R. J. Williams. Learning representations by back-propagating errors. *Nature*, 323(6088):533, 1986.

[42] T. N. Sainath and C. Parada. Convolutional neural networks for small-footprint keyword spotting. In *Sixteenth Annual Conference of the International Speech Communication Association*, 2015.

[43] Siri Team, Apple. Hey Siri: An on-device dnn-powered voice trigger for apple's personal assistant, 2017. URL https://machinelearning.apple.com/2017/10/01/hey-siri.html.

[44] R. K. Srivastava, K. Greff, and J. Schmidhuber. Highway networks. *arXiv preprint arXiv:1505.00387*, 2015.

[45] STCI, Microsoft. Wakeword dataset.

[46] G. A. Susto, A. Schirru, S. Pampuri, S. McLoone, and A. Beghi. Machine learning for predictive maintenance: A multiple classifier approach. *IEEE Transactions on Industrial Informatics*, 11 (3):812–820, 2015.

[47] E. Vorontsov, C. Trabelsi, S. Kadoury, and C. Pal. On orthogonality and learning recurrent networks with long term dependencies. In *International Conference on Machine Learning*, 2017.

[48] Z. Wang, J. Lin, and Z. Wang. Accelerating recurrent neural networks: A memory-efficient approach. *IEEE Transactions on Very Large Scale Integration (VLSI) Systems*, 25(10):2763–2775, 2017.

[49] P. Warden. Speech commands: A dataset for limited-vocabulary speech recognition. *arXiv preprint arXiv:1804.03209*, 2018. URL http://download.tensorflow.org/data/speech_commands_v0.01.tar.gz.

[50] S. Wisdom, T. Powers, J. Hershey, J. Le Roux, and L. Atlas. Full-capacity unitary recurrent neural networks. In *Advances in Neural Information Processing Systems*, pages 4880–4888, 2016.

[51] J. Ye, L. Wang, G. Li, D. Chen, S. Zhe, X. Chu, and Z. Xu. Learning compact recurrent neural networks with block-term tensor decomposition. *arXiv preprint arXiv:1712.05134*, 2017.

[52] Yelp Inc. Yelp dataset challenge, 2017. URL https://www.yelp.com/dataset/challenge.

[53] W. Zaremba, I. Sutskever, and O. Vinyals. Recurrent neural network regularization. *arXiv preprint arXiv:1409.2329*, 2014.

[54] J. Zhang, Q. Lei, and I. S. Dhillon. Stabilizing gradients for deep neural networks via efficient SVD parameterization. In *International Conference on Machine Learning*, 2018.

A Convergence Analysis for FastRNN

Algorithm 1: Randomized Stochastic Gradient

Input: Initial point θ_1, iteration limit M, step sizes $\gamma_{k\geq 1}$, Probability mass function $P_R(\cdot)$ supported on $\{1, 2, \ldots, M\}$

Initialize: R be a random variable with probability mass function P_R

for $m = 1, \ldots, R$ **do**

  Obtain sample of stochastic gradient $\nabla L_t(\theta_t)$

  $\theta_t \leftarrow \theta_{t-1} - \gamma_t \nabla L_t(\theta_t)$

Output: θ_R

Let $\theta = (\mathbf{W}, \mathbf{U}, \mathbf{v})$ represent the set of parameters of the scalar gated recurrent neural network. In order to prove the convergence properties of Randomized Stochastic Gradient (see Algorithm 1) as in [15], we first obtain a bound on the Lipschitz constant of the loss function $L(\mathbf{X}, y; \theta) := \log(1 + \exp(-y \cdot \mathbf{v}^\top \mathbf{h}_T))$ where $\mathbf{h}_T$ is the output of FastRNN after T time steps given input $\mathbf{X}$.

The gradient $\nabla_\theta L$ of the loss function is given by $(\frac{\partial L}{\partial \mathbf{W}}, \frac{\partial L}{\partial \mathbf{U}}, \frac{\partial L}{\partial \mathbf{v}})$ wherein

$$\frac{\partial L}{\partial \mathbf{U}} = \alpha \sum_{t=0}^{T} \mathbf{D}_t \left(\prod_{k=t}^{T-1} (\alpha \mathbf{U}^\top \mathbf{D}_{k+1} + \beta \mathbf{I}) \right) (\nabla_{\mathbf{h}_T} L) \mathbf{h}_{t-1}^\top \tag{9}$$

$$\frac{\partial L}{\partial \mathbf{W}} = \alpha \sum_{t=0}^{T} \mathbf{D}_t \left(\prod_{k=t}^{T-1} (\alpha \mathbf{U}^\top \mathbf{D}_{k+1} + \beta \mathbf{I}) \right) (\nabla_{\mathbf{h}_T} L) \mathbf{x}_t^\top \tag{10}$$

$$\frac{\partial L}{\partial \mathbf{v}} = \frac{-y \exp(-y \cdot \mathbf{v}^\top \mathbf{h}_T)}{1 + \exp(-y \cdot \mathbf{v}^\top \mathbf{h}_T)} \mathbf{h}_T, \tag{11}$$

where $\nabla_{\mathbf{h}_T} L = -c(\theta) y \cdot \mathbf{v}$, with $c(\theta) = \frac{1}{1+\exp(y \cdot \mathbf{v}^\top \mathbf{h}_T)}$. We do a perturbation analysis and obtain a bound on $\|\nabla_\theta L(\theta) - \nabla_\theta L(\theta + \delta)\|_2$ where $\delta = (\delta_{\mathbf{W}}, \delta_{\mathbf{U}}, \delta_{\mathbf{v}})$.

Deviation bound for $\mathbf{h}_T$: In this subsection, we consider bounding the term $\|\mathbf{h}_T(\theta + \delta) - \mathbf{h}_T(\theta)\|_2$ evaluated on the same input $\mathbf{X}$. Note that for FastRNN, $\mathbf{h}_T = \alpha \tilde{\mathbf{h}}_T + \beta \mathbf{h}_{T-1}$. For notational convenience, we use $\mathbf{h}'_T = \mathbf{h}_T(\theta + \delta)$ and $\mathbf{h}_T = \mathbf{h}_T(\theta)$.

$$\begin{aligned}
\|\mathbf{h}'_T - \mathbf{h}_T\|_2 &\leq \beta \|\mathbf{h}'_{T-1} - \mathbf{h}_{T-1}\|_2 + \alpha \|\sigma(\mathbf{W}\mathbf{x}_T + \mathbf{U}\mathbf{h}_{T-1}) - \sigma((\mathbf{W} + \delta_{\mathbf{W}})\mathbf{x}_T + (\mathbf{U} + \delta_{\mathbf{U}})\mathbf{h}'_{T-1})\|_2 \\
&\overset{\zeta_1}{\leq} \beta \|\mathbf{h}'_{T-1} - \mathbf{h}_{T-1}\|_2 + \alpha \|\mathbf{U}\mathbf{h}_{T-1} - \delta_{\mathbf{W}}\mathbf{x}_T - \mathbf{U}\mathbf{h}'_{T-1} - \delta_{\mathbf{U}}\mathbf{h}'_{T-1}\|_2 \\
&\leq (\alpha \|\mathbf{U}\|_2 + \beta) \|\mathbf{h}'_{T-1} - \mathbf{h}_{T-1}\|_2 + \alpha(\sqrt{\hat{D}} \cdot \|\delta_{\mathbf{U}}\|_2 + \|\delta_{\mathbf{W}}\|_2 R_{\mathbf{x}}) \\
&\vdots \\
&\leq \alpha(\sqrt{\hat{D}} \cdot \|\delta_{\mathbf{U}}\|_2 + \|\delta_{\mathbf{W}}\|_2 R_{\mathbf{x}}) \left(1 + (\alpha \|\mathbf{U}\|_2 + \beta) + \ldots + (\alpha \|\mathbf{U}\|_2 + \beta)^{T-1}\right) \\
&\overset{\zeta_2}{\leq} \alpha(\sqrt{\hat{D}} \cdot \|\delta_{\mathbf{U}}\|_2 + \|\delta_{\mathbf{W}}\|_2 R_{\mathbf{x}}) \frac{(\alpha(\|\mathbf{U}\|_2 - 1) + 1)^T - 1}{\alpha(\|\mathbf{U}\|_2 - 1)} \leq 2\alpha(\sqrt{\hat{D}} \cdot \|\delta_{\mathbf{U}}\|_2 + \|\delta_{\mathbf{W}}\|_2 R_{\mathbf{x}}) \cdot T \\
&\leq \frac{2\sqrt{\hat{D}} \cdot \|\delta_{\mathbf{U}}\|_2 + 2\|\delta_{\mathbf{W}}\|_2 R_{\mathbf{x}}}{|\|\mathbf{U}\|_2 - 1|},
\end{aligned} \tag{12}$$

where ζ_1 follows by using 1-lipschitz property of the sigmoid function and ζ_2 follows by setting $\alpha = O(\frac{1}{T \cdot |\|\mathbf{U}\|_2 - 1|})$ and $\beta = 1 - \alpha$.

Deviation bound for $c(\theta)$: In this subsection, we consider bounding the deviation $c(\theta) - c(\theta + \delta)$.

$$\begin{aligned}
|c(\theta) - c(\theta + \delta)| &\leq |\mathbf{v}^\top \mathbf{h}_T - (\mathbf{v} + \delta_{\mathbf{v}}^\top)\mathbf{h}'_T| \\
&\leq |\mathbf{v}^\top (\mathbf{h}_T - \mathbf{h}'_T)| + \|\delta_{\mathbf{v}}\|_2 \|\mathbf{h}_t\|_2 \\
&\leq \|\mathbf{v}\|_2 \|\mathbf{h}_T - \mathbf{h}'_T\|_2 + \|\delta_{\mathbf{v}}\|_2 \|\mathbf{h}_t\|_2 \\
&\leq R_{\mathbf{v}} \|\mathbf{h}_T - \mathbf{h}'_T\|_2 + \sqrt{\hat{D}} \|\delta_{\mathbf{v}}\|_2.
\end{aligned} \tag{13}$$

Deviation bound for $\frac{\partial L}{\partial \mathbf{v}}$: In this subsection we consider the bounds on $\|\frac{\partial L}{\partial \mathbf{v}}(\theta) - \frac{\partial L}{\partial \mathbf{v}}(\theta+\delta)\|_2$.

$$\begin{aligned}
\left\|\frac{\partial L}{\partial \mathbf{v}}(\theta) - \frac{\partial L}{\partial \mathbf{v}}(\theta+\delta)\right\|_2 &= \left\|\frac{\mathbf{h}_T}{1+\exp\left(y\mathbf{v}^\top \mathbf{h}_T\right)} - \frac{\mathbf{h}'_T}{1+\exp\left(y(\mathbf{v}+\delta_\mathbf{v})^\top \mathbf{h}'_T\right)}\right\|_2 \\
&= \left\|c(\theta)\mathbf{h}_T - c(\theta+\delta)\mathbf{h}'_T)\right\|_2 \\
&= \|(c(\theta)-c(\theta+\delta))\cdot \mathbf{h}_T + c(\theta+\delta)\cdot(\mathbf{h}_T - \mathbf{h}'_T)\|_2 \\
&\leq \sqrt{\hat{D}}\cdot|c(\theta)-c(\theta+\delta)| + \|\mathbf{h}_T - \mathbf{h}'_T\|_2 \\
&\leq \left(\sqrt{\hat{D}}R_\mathbf{v}+1\right)\cdot\|\mathbf{h}_T-\mathbf{h}'_T\|_2 + \hat{D}\|\delta_\mathbf{v}\|_2. \qquad (14)
\end{aligned}$$

Deviation bound for $\frac{\partial L}{\partial \mathbf{W}}$: In this subsection, we analyze $\|\frac{\partial L}{\partial \mathbf{W}}(\theta) - \frac{\partial L}{\partial \mathbf{W}}(\theta+\delta)\|_2$. Let $\mathcal{D} = \sup_{k,\theta}\|\mathbf{D}_k^\theta\|$.

$$\begin{aligned}
&\left\|\frac{\partial L}{\partial \mathbf{W}}(\theta) - \frac{\partial L}{\partial \mathbf{W}}(\theta+\delta)\right\|_F \\
&= \alpha R_\mathbf{x}\left\|\sum_{t=0}^{T}\left[\left(c(\theta)\mathbf{D}_t^\theta\prod_{k=t}^{T-1}(\alpha\mathbf{U}^\top\mathbf{D}_{k+1}^\theta+\beta\mathbf{I})\right)\mathbf{v} - \left(c(\theta+\delta)\mathbf{D}_t^{\theta+\delta}\prod_{k=t}^{T-1}(\alpha(\mathbf{U}+\delta_\mathbf{U})^\top\mathbf{D}_{k+1}^{\theta+\delta}+\beta\mathbf{I})\right)(\mathbf{v}+\delta_\mathbf{v})\right]\right\|_2. \qquad (15)
\end{aligned}$$

Let us define matrices $\mathcal{A}_t^\theta := \mathbf{D}_t^\theta\prod_{k=t}^{T-1}(\alpha\mathbf{U}^\top\mathbf{D}_{k+1}^\theta + \beta\mathbf{I})$ and similarly $\mathcal{A}_t^{\theta+\delta} := \mathbf{D}_t^{\theta+\delta}\prod_{k=t}^{T-1}(\alpha(\mathbf{U}+\delta_\mathbf{U})^\top\mathbf{D}_{k+1}^{\theta+\delta}+\beta\mathbf{I})$. Using this, we have,

$$\begin{aligned}
&\left\|\frac{\partial L}{\partial \mathbf{W}}(\theta) - \frac{\partial L}{\partial \mathbf{W}}(\theta+\delta)\right\|_F \\
&= \alpha R_\mathbf{x}\left\|\sum_{t=0}^{T}\left[c(\theta)\cdot\mathcal{A}_t^\theta\mathbf{v} - c(\theta+\delta)\cdot\mathcal{A}_t^{\theta+\delta}(\mathbf{v}+\delta_\mathbf{v})\right]\right\|_2 \\
&\leq \alpha R_\mathbf{x}\left(|c(\theta)-c(\theta+\delta)|\cdot\left\|\sum_{t=0}^{T}\mathcal{A}_t^\theta\mathbf{v}\right\|_2 + \left\|\sum_{t=0}^{T}\mathcal{A}_t^\theta\mathbf{v} - \mathcal{A}_t^{\theta+\delta}(\mathbf{v}+\delta_\mathbf{v})\right\|_2\right) \\
&\leq \alpha R_\mathbf{x}\left(|c(\theta)-c(\theta+\delta)|\cdot\left\|\sum_{t=0}^{T}\mathcal{A}_t^\theta\mathbf{v}\right\|_2 + \left\|\sum_{t=0}^{T}(\mathcal{A}_t^\theta - \mathcal{A}_t^{\theta+\delta})\mathbf{v}\right\|_2 + \left\|\sum_{t=0}^{T}\mathcal{A}_t^{\theta+\delta}\delta_\mathbf{v}\right\|_2\right) \\
&\leq \alpha R_\mathbf{x}\left(|c(\theta)-c(\theta+\delta)|\cdot R_\mathbf{v}\left\|\sum_{t=0}^{T}\mathcal{A}_t^\theta\right\|_2 + R_\mathbf{v}\left\|\sum_{t=0}^{T}\mathcal{A}_t^\theta - \mathcal{A}_t^{\theta+\delta}\right\|_2 + \|\delta_\mathbf{v}\|_2\left\|\sum_{t=0}^{T}\mathcal{A}_t^{\theta+\delta}\right\|_2\right). \qquad (16)
\end{aligned}$$

We will proceed by bounding the first term in the above equation. Consider,

$$\begin{aligned}
\left\|\sum_{t=0}^{T}\mathcal{A}_t^\theta\right\|_2 &\leq \mathcal{D}\sum_{t=0}^{T}\left\|\prod_{k=t}^{T-1}(\alpha\mathbf{U}^\top\mathbf{D}_{k+1}^\theta+\beta\mathbf{I})\right\|_2 \\
&\leq \mathcal{D}\sum_{t=0}^{T}(\alpha\mathcal{D}\cdot\|\mathbf{U}\|_2+\beta)^{T-t} \\
&\leq \mathcal{D}\frac{|(\alpha\mathcal{D}\cdot\|\mathbf{U}\|_2+\beta)^{T+1}-1|}{|\alpha\mathcal{D}\cdot\|\mathbf{U}\|_2+\beta-1|} \\
&\overset{\zeta_1}{\leq} \mathcal{D}\frac{(1+\alpha\cdot(\mathcal{D}\|U\|_2-1))^{T+1}-1}{\alpha|\mathcal{D}\|\mathbf{U}\|_2-1|} \\
&\overset{\zeta_2}{\leq} 2\mathcal{D}\cdot(T+1), \qquad (17)
\end{aligned}$$

where ζ_1 follows by setting $\beta = 1-\alpha$ and ζ_2 follows by using the inequality $(1+x)^r \leq 1+2rx$ for $(r-1)x \leq 1/2$ and the fact that $\alpha \leq \frac{1}{4T\cdot|\mathcal{D}\|U\|_2-1|}$. Note that the third term in Equation (17) can be bounded in a similar way as above by $2\mathcal{D}\cdot(T+1)$ using $\alpha \leq \frac{1}{4T\cdot R_\mathbf{U}}$. We now proceed to

bound the second term. Consider the following for any fixed value of t,

$$\begin{aligned}
\left\|\mathcal{A}_t^\theta - \mathcal{A}_t^{\theta+\delta}\right\|_2 &= \left\|\mathbf{D}_t^\theta \prod_{k=t}^{T-1}(\alpha \mathbf{U}^\top \mathbf{D}_{k+1}^\theta + \beta \mathbf{I}) - \mathbf{D}_t^{\theta+\delta} \prod_{k=t}^{T-1}(\alpha(\mathbf{U}+\delta_\mathbf{U})^\top \mathbf{D}_{k+1}^{\theta+\delta} + \beta \mathbf{I})\right\|_2 \\
&\le \left\|(\mathbf{D}_t^\theta - \mathbf{D}_t^{\theta+\delta}) \prod_{k=t}^{T-1}(\alpha \mathbf{U}^\top \mathbf{D}_{k+1}^\theta + \beta \mathbf{I})\right\|_2 + \mathcal{D}\left\|\prod_{k=t}^{T-1}(\alpha \mathbf{U}^\top \mathbf{D}_{k+1}^\theta + \beta \mathbf{I}) - \prod_{k=t}^{T-1}(\alpha(\mathbf{U}+\delta_\mathbf{U})^\top \mathbf{D}_{k+1}^{\theta+\delta} + \beta \mathbf{I})\right\|_2 \\
&\le \left\|\mathbf{D}_t^\theta - \mathbf{D}_t^{\theta+\delta}\right\|_2 \cdot \left\|\prod_{k=t}^{T-1}(\alpha \mathbf{U}^\top \mathbf{D}_{k+1}^\theta + \beta \mathbf{I})\right\|_2 + \mathcal{D}\left\|\prod_{k=t}^{T-1}(\alpha \mathbf{U}^\top \mathbf{D}_{k+1}^\theta + \beta \mathbf{I}) - \prod_{k=t}^{T-1}(\alpha(\mathbf{U}+\delta_\mathbf{U})^\top \mathbf{D}_{k+1}^{\theta+\delta} + \beta \mathbf{I})\right\|_2 \\
&\le \left\|\mathbf{D}_t^\theta - \mathbf{D}_t^{\theta+\delta}\right\|_2 \cdot (\alpha\|\mathbf{U}\|_2\mathcal{D} + \beta)^{T-t} + \mathcal{D}\underbrace{\left\|\prod_{k=t}^{T-1}(\alpha \mathbf{U}^\top \mathbf{D}_{k+1}^\theta + \beta \mathbf{I}) - \prod_{k=t}^{T-1}(\alpha(\mathbf{U}+\delta_\mathbf{U})^\top \mathbf{D}_{k+1}^{\theta+\delta} + \beta \mathbf{I})\right\|_2}_{(I)}.
\end{aligned}$$

Let $\Delta_k^\theta := \mathbf{D}_k^\theta - \mathbf{D}_k^{\theta+\delta}$. We will later show that $\left\|\Delta_k^\theta\right\|_2 \le \Delta_\theta$ independent of the value of k. We focus on term (I) in the expression above:

$$\begin{aligned}
&\left\|\prod_{k=t}^{T-1}(\alpha \mathbf{U}^\top \mathbf{D}_{k+1}^\theta + \beta \mathbf{I}) - \prod_{k=t}^{T-1}(\alpha(\mathbf{U}+\delta_\mathbf{U})^\top \mathbf{D}_{k+1}^{\theta+\delta} + \beta \mathbf{I})\right\|_2 \\
&\quad\le \left\|\prod_{k=t}^{T-1}(\alpha \mathbf{U}^\top \mathbf{D}_{k+1}^{\theta+\delta} + \beta \mathbf{I} + \alpha \mathbf{U}^\top \Delta_{k+1}^\theta) - \prod_{k=t}^{T-1}(\alpha \mathbf{U}^\top \mathbf{D}_{k+1}^{\theta+\delta} + \beta \mathbf{I} + \alpha \delta_\mathbf{U}^\top \mathbf{D}_{k+1}^{\theta+\delta})\right\|_2. \qquad (18)
\end{aligned}$$

Let $\mathcal{B}_k := \alpha \mathbf{U}^\top \mathbf{D}_k^{\theta+\delta} + \beta \mathbf{I}$, $\mathcal{C}_k := \alpha \mathbf{U}^\top \Delta_{k+1}^\theta$ and $\mathcal{G}_k := \alpha \delta_\mathbf{U}^\top \mathbf{D}_{k+1}^{\theta+\delta}$. Note that we have the following bounds on the operator norms of these matrices:

$$\|\mathcal{B}_k\|_2 \le \alpha\mathcal{D}\cdot\|\mathbf{U}\|_2 + \beta = \mathcal{B}_{\max}, \quad \|\mathcal{C}_k\|_2 \le \alpha\Delta_\theta \cdot \|\mathbf{U}\|_2 = \mathcal{C}_{\max}, \quad \|\mathcal{G}_k\| \le \alpha\mathcal{D}\cdot\|\delta_\mathbf{U}\|_2 = \mathcal{G}_{\max}. \qquad (19)$$

By our assumptions on α, $\mathcal{B}_k$ is invertible and $I + \mathcal{B}_k\mathcal{C}_k\mathcal{B}_k^{-1}$, $I + \mathcal{B}_k\mathcal{G}_k\mathcal{B}_k^{-1}$ are diagonizable. Moreover, $\|\mathcal{B}_k^{-1}\| \le 2\alpha\mathcal{D}\cdot\|\mathbf{U}\|_2 + \beta = \mathcal{B}_{\max}^{-1}$.

Hence, we can rewrite Equation (18) as,

$$\begin{aligned}
&\left\|\prod_{k=t}^{T-1}(\alpha \mathbf{U}^\top \mathbf{D}_{k+1}^\theta + \beta \mathbf{I}) - \prod_{k=t}^{T-1}(\alpha(\mathbf{U}+\delta_\mathbf{U})^\top \mathbf{D}_{k+1}^{\theta+\delta} + \beta \mathbf{I})\right\|_2 \\
&\quad\le \left\|\prod_{k=t}^{T-1}(\mathcal{B}_k + \mathcal{C}_k) - \prod_{k=t}^{T-1}(\mathcal{B}_k + \mathcal{G}_k)\right\| \\
&\quad\le 4\|\mathcal{B}_t\| \cdot \left\|\prod_{k=t}^{T-1}\left(I + \mathcal{B}_t^{-1}\mathcal{C}_k\mathcal{B}_{t+1}\right) - \prod_{k=t}^{T-1}\left(I + \mathcal{B}_t^{-1}\mathcal{G}_k\mathcal{B}_{t+1}\right)\right\| \\
&\quad\le 4\|\mathcal{B}_t\| \cdot \left((1 + \mathcal{B}_{\max}\cdot\mathcal{C}_{\max}\cdot\mathcal{B}_{\max}^{-1})^{T-t} - 1 + (1 + \mathcal{B}_{\max}\cdot\mathcal{G}_{\max}\cdot\mathcal{B}_{\max}^{-1})^{T-t} - 1\right), \qquad (20)
\end{aligned}$$

where $B_T := I$ and the last equation follows from the following fact: $\|\prod_{k=1}^T(I + C_k) - I\| \le (\max_k \|C_k\| + 1)^T - 1$.

Combining the above term with Equation (16):

$$\begin{aligned}
\left\|\sum_{t=0}^T \mathcal{A}_t^\theta - \mathcal{A}_t^{\theta+\delta}\right\|_2 &\le \sum_{t=0}^T \left\|\mathcal{A}_t^\theta - \mathcal{A}_t^{\theta+\delta}\right\|_2 \\
&\le \Delta_\theta \cdot \sum_{t=0}^T (\alpha\mathcal{D}\cdot\|\mathbf{U}\|_2 + \beta)^{T-t} + \mathcal{D}\cdot\mathcal{B}_{\max}^{-1}\cdot\mathcal{B}_{\max} \\
&\quad\cdot \sum_{t=0}^T \left((1 + \mathcal{B}_{\max}\cdot\mathcal{C}_{\max}\cdot\mathcal{B}_{\max}^{-1})^{T-t} - 1 + (1 + \mathcal{B}_{\max}\cdot\mathcal{G}_{\max}\cdot\mathcal{B}_{\max}^{-1})^{T-t} - 1\right) \\
&\le \Delta_\theta \cdot \sum_{t=0}^T (\alpha\mathcal{D}\cdot\|\mathbf{U}\|_2 + \beta)^{T-t} + 2\mathcal{D}\cdot(\mathcal{B}_{\max}^{-1})^3\cdot(\mathcal{B}_{\max})^3\cdot T^2\cdot((\mathcal{C}_{\max})^2 + (\mathcal{G}_{\max})^2) \\
&\overset{\zeta_1}{\le} 2\Delta_\theta\cdot(T+1) + 2\mathcal{D}\cdot(\mathcal{B}_{\max}^{-1})^3\cdot(\mathcal{B}_{\max})^3\cdot T^2\cdot((\mathcal{C}_{\max})^2 + (\mathcal{G}_{\max})^2), \qquad (21)
\end{aligned}$$

where ζ_1 follows by summing the geometric series and using the fact that $\alpha \leq \frac{1}{4T\cdot|\mathcal{D}\|U\|_2-1|}$.

Using the definition of $D_k^\theta = \text{diag}(\sigma'(\mathbf{W}\mathbf{x}_k + \mathbf{U}\mathbf{h}_{k-1}))$ from Section 3 of the paper, we obtain a bound on Δ_k^θ.

$$\begin{aligned}\left\|\mathbf{D}_k^\theta - \mathbf{D}_k^{\theta+\delta}\right\|_2 &\leq 2\left(R_{\mathbf{x}}\cdot\|\delta_{\mathbf{W}}\|_2 + \sqrt{\hat{D}}\cdot\|\delta_{\mathbf{U}}\|_2 + R_{\mathbf{U}}\cdot\|\mathbf{h}_{k-1}-\mathbf{h}'_{k-1}\|_2\right)\\ &\overset{\zeta_1}{\leq} 2\left(R_{\mathbf{x}}\cdot\|\delta_{\mathbf{W}}\|_2 + \sqrt{\hat{D}}\cdot\|\delta_{\mathbf{U}}\|_2 + R_{\mathbf{U}}\cdot\frac{2\sqrt{\hat{D}}\cdot\|\delta_{\mathbf{U}}\|_2 + 2\|\delta_{\mathbf{W}}\|_2 R_{\mathbf{x}}}{|\|U\|_2-1|}\right), \end{aligned} \tag{22}$$

where ζ_1 follows from using the bound from Equation (12). Combining bounds obtained in Equations (16), (17), (21) and (22), we obtain that,

$$\left\|\frac{\partial L}{\partial \mathbf{W}}(\theta) - \frac{\partial L}{\partial \mathbf{W}}(\theta+\delta)\right\|_F \leq \mathcal{O}(\alpha T)\cdot\|\delta\|_F, \quad \text{for}$$
$$\alpha \leq \min\left(\frac{1}{4T\cdot|\mathcal{D}\|U\|_2-1|}, \frac{1}{4T\cdot R_{\mathbf{U}}}, \frac{1}{2T\cdot\Delta_\theta\|U\|_2}, \frac{1}{T\cdot|\|\mathbf{U}\|_2-1|}\right)$$

where the $\mathcal{O}$ notation hides *polynomial* dependence of the Lipschitz smoothness constant of L on $R_{\mathbf{W}}, R_{\mathbf{U}}, R_{\mathbf{v}}, R_{\mathbf{x}}, \|\mathbf{U}\|_2, \|\mathbf{W}\|_2$ and the ambient dimensions $D, \hat{D}$.

Deviation bound for $\frac{\partial L}{\partial \mathbf{U}}$: Following similar arguments as we did above for $\frac{\partial L}{\partial \mathbf{W}}$, we can derive the perturbation bound for the term $\frac{\partial L}{\partial \mathbf{U}}$ as

$$\left\|\frac{\partial L}{\partial \mathbf{U}}(\theta) - \frac{\partial L}{\partial \mathbf{U}}(\theta+\delta)\right\|_F = \mathcal{O}(\alpha T)\cdot\|\delta\|_F \tag{23}$$

where the $\mathcal{O}$ notation is the same as above.

Using our bounds in corollary 2.2 of [15], we obtain the following convergence theorem.

Theorem 3.1 (Convergence Bound)**.** *Let $[(\mathbf{X}_1, y_1), \ldots, (\mathbf{X}_n, y_n)]$ be the given labeled sequential training data. Let $L(\theta) = \frac{1}{n}\sum_i L(\mathbf{X}_i, y_i; \theta)$ be the loss function with $\theta = (\mathbf{W}, \mathbf{U}, \mathbf{v})$ be the parameters of FastRNN architecture (2) with $\beta = 1-\alpha$ and α such that*

$$\alpha \leq \min\left(\frac{1}{4T\cdot|\mathcal{D}\|\mathbf{U}\|_2-1|}, \frac{1}{4T\cdot R_{\mathbf{U}}}, \frac{1}{2T\cdot\Delta_\theta\|\mathbf{U}\|_2}, \frac{1}{T\cdot|\|\mathbf{U}\|_2-1|}\right),$$

where $\mathcal{D} = \sup_{\theta,k}\|\mathbf{D}_k^\theta\|_2$. Then, randomized stochastic gradient descent [15], a minor variation of SGD, when applied to the data for a maximum of M iteration outputs a solution $\widehat{\theta}$ such that:

$$\mathbb{E}[\|\nabla_\theta L(\widehat{\theta})\|_2^2\|] \leq \mathcal{B}_M := \frac{\mathcal{O}(\alpha T)L(\theta_0)}{M} + \left(\bar{D} + \frac{4R_{\mathbf{W}}R_{\mathbf{U}}R_{\mathbf{v}}}{\bar{D}}\right)\frac{\mathcal{O}(\alpha T)}{\sqrt{M}},$$

where $R_{\mathbf{X}} = \max_{\mathbf{X}}\|\mathbf{X}\|_F$ for $\mathbf{X} = \{\mathbf{U}, \mathbf{W}, \mathbf{v}\}$, $L(\theta_0)$ is the loss of the initial classifier, and the step-size of the k-th SGD iteration is fixed as: $\gamma_k = \min\left\{\frac{1}{\mathcal{O}(\alpha T)}, \frac{\bar{D}}{T\sqrt{M}}\right\}, k \in [M],\ \bar{D} \geq 0$.

A.1 Generalization Bound for FastRNN

In this subsection, we compute the Rademacher complexity of the class of real valued scalar gated recurrent neural networks such that $\|\mathbf{U}\|_F \leq R_{\mathbf{U}}, \|\mathbf{W}\|_F \leq R_{\mathbf{W}}$. Also the input $\mathbf{x}_t$ at time step t is assumed to be point-wise bounded $\|\mathbf{x}_t\|_2 \leq R_{\mathbf{x}}$ The update equation of FastRNN is given by

$$\mathbf{h}_t = \alpha\sigma(\mathbf{W}\mathbf{x}_t + \mathbf{U}\mathbf{h}_{t-1}) + \beta\mathbf{h}_{t-1}.$$

For the purpose of this section, we use the shorthand $\mathbf{h}_t^i$ to denote the hidden vector at time t corresponding to the i^{th} data point $\mathbf{X}^i$. We denote the Rademacher complexity of a T layer FastRNN

by $\mathcal{R}_n(\mathcal{F}_T)$ evaluated using n data points.

$$
\begin{aligned}
n\mathcal{R}_n(\mathcal{F}_T) &= \mathbb{E}_\epsilon \left[\sup_{\mathbf{W},\mathbf{U}} \left\| \sum_{i=1}^{n} \epsilon_i \mathbf{h}_T^i \right\| \right] \\
&= \mathbb{E}_\epsilon \left[\sup_{\mathbf{W},\mathbf{U}} \left\| \sum_{i=1}^{n} \epsilon_i \left(\alpha\sigma(\mathbf{W}\mathbf{x}_T^i + \mathbf{U}\mathbf{h}_{T-1}^i) + \beta \mathbf{h}_{T-1}^i \right) \right\| \right] \\
&\overset{\zeta_1}{\leq} \mathbb{E}_\epsilon \left[\sup_{\mathbf{W},\mathbf{U}} \beta \left\| \sum_{i=1}^{n} \epsilon_i \mathbf{h}_{T-1}^i \right\| \right] + \mathbb{E}_\epsilon \left[\sup_{\mathbf{W},\mathbf{U}} \alpha \left\| \sum_{i=1}^{n} \epsilon_i (\sigma(\mathbf{W}\mathbf{x}_T^i + \mathbf{U}\mathbf{h}_{T-1}^i)) \right\| \right] \\
&\overset{\zeta_2}{\leq} \beta \mathcal{R}_n(\mathcal{F}_{T-1}) + 2\mathbb{E}_\epsilon \left[\sup_{\mathbf{W},\mathbf{U}} \alpha \left\| \sum_{i=1}^{n} \epsilon_i (\mathbf{W}\mathbf{x}_T^i + \mathbf{U}\mathbf{h}_{T-1}^i) \right\| \right] \\
&\overset{\zeta_3}{\leq} \beta \mathcal{R}_n(\mathcal{F}_{T-1}) + 2\alpha\mathbb{E}_\epsilon \left[\sup_{W} \left\| \sum_{i=1}^{n} \epsilon_i \mathbf{W}\mathbf{x}_T^i \right\| \right] + 2\alpha\mathbb{E}_\epsilon \left[\sup_{\mathbf{W},\mathbf{U}} \left\| \sum_{i=1}^{n} \epsilon_i \mathbf{U}\mathbf{h}_{T-1}^i) \right\| \right] \\
&\overset{\zeta_4}{\leq} \beta \mathcal{R}_n(\mathcal{F}_{T-1}) + 2\alpha R_{\mathbf{W}} \mathbb{E}_\epsilon \left[\left\| \sum_{i=1}^{n} \epsilon_i \mathbf{x}_T^i \right\| \right] + 2\alpha R_{\mathbf{U}} \mathbb{E}_\epsilon \left[\sup_{\mathbf{W},\mathbf{U}} \left\| \sum_{i=1}^{n} \epsilon_i \mathbf{h}_{T-1}^i) \right\| \right] \\
&\leq (\beta + 2\alpha R_{\mathbf{U}}) \mathcal{R}_n(\mathcal{F}_{T-1}) + 2\alpha R_{\mathbf{W}} R_{\mathbf{X}} \sqrt{n} \\
&\leq (\beta + 2\alpha R_{\mathbf{U}})^2 \mathcal{R}_n(\mathcal{F}_{T-2}) + 2\alpha R_{\mathbf{W}} R_{\mathbf{X}} \sqrt{n} (1 + (\beta + 2\alpha R_{\mathbf{U}})) \\
&\vdots \\
&\leq 2\alpha R_{\mathbf{W}} R_{\mathbf{X}} \sum_{t=0}^{T-1} (\beta + 2\alpha R_{\mathbf{U}})^{T-t} \sqrt{n} \\
&\leq 2\alpha R_{\mathbf{W}} R_{\mathbf{X}} \left(\frac{(\beta + 2\alpha R_{\mathbf{U}})^{T+1} - 1}{(\beta + 2\alpha R_{\mathbf{U}}) - 1} \right) \sqrt{n} \\
&\leq 2\alpha R_{\mathbf{W}} R_{\mathbf{X}} \left(\frac{(1 + \alpha(2R_U - 1))^{T+1} - 1}{\alpha(2R_{\mathbf{U}} - 1)} \right) \sqrt{n} \\
&\overset{\zeta_5}{\leq} 2R_{\mathbf{W}} R_{\mathbf{X}} \left(\frac{2\alpha(2R_{\mathbf{U}} - 1)(T+1)}{(2R_{\mathbf{U}} - 1)} \right) \sqrt{n},
\end{aligned}
$$

where ζ_1, ζ_3 follows by triangle inequality and noting that the terms in the sum of expectation are pointwise bigger than the previous term, ζ_2 follows from the Ledoux-Talagrand contraction, ζ_4 follows using an argument similar from Lemma 1 in [16] and ζ_5 holds for $\alpha \leq \frac{1}{2(2R_{\mathbf{U}}-1)T}$.

Theorem 3.2 (Generalization Error Bound)**.** *[6] Let $\mathcal{Y}, \hat{\mathcal{Y}} \subseteq [0,1]$ and let $\mathcal{F}_T$ denote the class of FastRNN with $\|\mathbf{U}\|_F \leq R_{\mathbf{U}}, \|\mathbf{W}\|_F \leq R_{\mathbf{W}}$. Let the final classifier be given by $\sigma(\mathbf{v}^\top \mathbf{h}_T)$, $\|\mathbf{v}\|_2 \leq R_{\mathbf{v}}$. Let $L : \mathcal{Y} \times \hat{\mathcal{Y}} \to [0, B]$ be any 1-Lipschitz loss function. Let D be any distribution on $\mathcal{X} \times \mathcal{Y}$ such that $\|\mathbf{x}_{it}\|_2 \leq R_x$ a.s. Let $0 \leq \delta \leq 1$. For all $\beta = 1 - \alpha$ and alpha such that,*

$$
\alpha \leq \min \left(\frac{1}{4T \cdot |\mathcal{D}\|\mathbf{U}\|_2 - 1|}, \frac{1}{4T \cdot R_{\mathbf{U}}}, \frac{1}{T \cdot |\|\mathbf{U}\|_2 - 1|} \right).
$$

where $\mathcal{D} = \sup_{\theta,k} \|\mathbf{D}_k^\theta\|_2$, we have that with probability at least $1 - \delta$, all functions $f \in \mathbf{v} \circ \mathcal{F}_T$ satisfy,

$$
\mathbb{E}_D[L(f(\mathbf{X}), y)] \leq \frac{1}{n} \sum_{i=1}^{n} L(f(\mathbf{X}_i), y_i) + \mathcal{C} \frac{O(\alpha T)}{\sqrt{n}} + B\sqrt{\frac{\ln(\frac{1}{\delta})}{n}},
$$

where $\mathcal{C} = R_{\mathbf{W}} R_{\mathbf{U}} R_{\mathbf{x}} R_{\mathbf{v}}$ represents the boundedness of the parameter matrices and the data.

The Rademacher complexity bounds for the function class $\mathcal{F}_T$ have been instantiated from the calculations above.

B Dataset Information

Google-12 & Google-30: Google Speech Commands dataset contains 1 second long utterances of 30 short words (30 classes) sampled at 16KHz. Standard log Mel-filter-bank featurization with 32 filters over a window size of 25ms and stride of 10ms gave 99 timesteps of 32 filter responses for a 1-second audio clip. For the 12 class version, 10 classes used in Kaggle's Tensorflow Speech Recognition challenge[1] were used and remaining two classes were noise and background sounds (taken randomly from remaining 20 short word utterances). Both the datasets were zero mean - unit variance normalized during training and prediction.

Wakeword-2: Wakeword-2 consists of 1.63 second long utterances sampled at 16KHz. This dataset was featurized in the same way as the Google Speech Commands dataset and led to 162 timesteps of 32 filter responses. The dataset was zero mean - unit variance normalized during training and prediction.

HAR-2[2]: Human Activity Recognition (HAR) dataset was collected from an accelerometer and gyroscope on a Samsung Galaxy S3 smartphone. The features available on the repository were directly used for experiments. The 6 activities were merged to get the binarized version. The classes {Sitting, Laying, Walking_Upstairs} and {Standing, Walking, Walking_Downstairs} were merged to obtain the two classes. The dataset was zero mean - unit variance normalized during training and prediction.

DSA-19[3]: This dataset is based on Daily and Sports Activity (DSA) detection from a resource-constrained IoT wearable device with 5 Xsens MTx sensors having accelerometers, gyroscopes and magnetometers on the torso and four limbs. The features available on the repository were used for experiments. The dataset was zero mean - unit variance normalized during training and prediction.

Yelp-5: Sentiment Classification dataset based on the text reviews[4]. The data consists of 500,000 train points and 500,000 test points from the first 1 million reviews. Each review was clipped or padded to be 300 words long. The vocabulary consisted of 20000 words and 128 dimensional word embeddings were jointly trained with the network.

Penn Treebank: 300 length word sequences were used for word level language modeling task using Penn Treebank (PTB) corpus. The vocabulary consisted of 10,000 words and the size of trainable word embeddings was kept the same as the number of hidden units of architecture.

Pixel-MNIST-10: Pixel-by-pixel version of the standard MNIST-10 dataset [5].The dataset was zero mean - unit variance normalized during training and prediction.

AmazonCat-13K [34, 8]: AmazonCat-13K is an extreme multi-label classification dataset with 13,330 labels. The raw text from title and content for Amazon products was provided as an input with each product being assigned to multiple categories. The input text was clipped or padded to ensure that it was 500 words long with a vocabulary of size 267,134. The 50 dimensional trainable word embeddings were initialized with GloVe vectors trained on Wikipedia.

Evaluation on Multilabel Dataset

The models were trained on the AmazonCat-13K dataset using Adam optimizer with a learning rate of 0.009 and batch size of 128. Binary Cross Entropy loss was used where the output of each neuron corresponds to the probability of a label being positive. 128 hidden units were chosen across architectures and were trained using PyTorch framework.

The results in Table 6 show that FastGRNN-LSQ achieves classification performance similar to state-of-the-art gated architectures (GRU, LSTM) while still having 2-3x lower memory footprint. Note that the model size reported doesn't include the embeddings and the final linear classifier which are memory intensive when compared to the model itself. FastRNN, as shown in the earlier

[1] https://www.kaggle.com/c/tensorflow-speech-recognition-challenge

[2] https://archive.ics.uci.edu/ml/datasets/human+activity+recognition+using+smartphones

[3] https://archive.ics.uci.edu/ml/datasets/Daily+and+Sports+Activities

[4] https://www.yelp.com/dataset/challenge

[5] http://yann.lecun.com/exdb/mnist/

Table 6: Extreme Multi Label Classification

Dataset	AmazonCat - 13K					
	P@1	P@2	P@3	P@4	P@5	Model Size - RNN (KB)
GRU	92.82	85.18	77.09	69.42	61.85	268
RNN	40.24	28.13	22.83	20.29	18.25	89.5
FastGRNN-LSQ	92.66	84.67	76.19	66.67	60.63	90.0
FastRNN	91.03	81.75	72.37	64.13	56.81	89.5
UGRNN	92.84	84.93	76.33	68.27	60.63	179

experiments, stabilizes standard RNN and achieves an improvement of over 50% in classification accuracy (P@1).

C Supplementary Experiments

Accuracy vs Model Size: This paper evaluates the trade-off between model size (in the range 0-128Kb) and accuracy across various architectures.

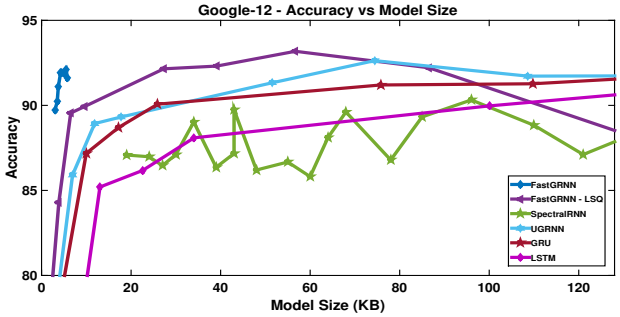

Figure 3: Accuracy vs Model Size

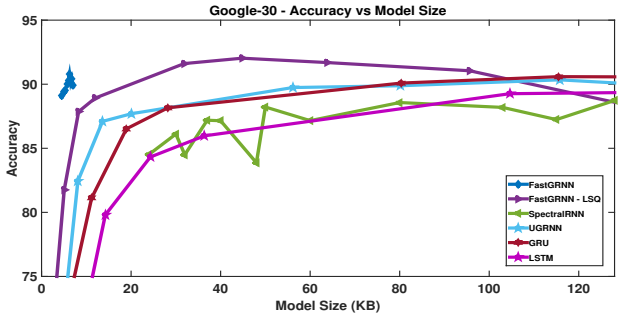

Figure 4: Accuracy vs Model Size

Figures 3, 4 show the plots for analyzing the model-size vs accuracy trade-off for FastGRNN, FastGRNN-LSQ along with leading unitary method SpectralRNN and the gated methods like UGRNN, GRU, and LSTM. FastGRNN is able to achieve state-of-the-art accuracies on Google-12 and Google-30 datasets at significantly lower model sizes as compared to other baseline methods.

Bias due to the initial hidden states: In order to understand the bias induced at the output by the initial hidden state h_0, we evaluated a trained FastRNN classifier on the Google-12 dataset with 3 different initializations sampled from a standard normal distribution. The resulting accuracies had a mean value of 92.08 with a standard deviation of 0.09, indicating that the initial state does not induce a bias in FastRNN prediction in the learning setting. In the non-learning setting, the initial

state can bias the final solution for very small values of α. Indeed, setting $\alpha = 0$ and $\beta = 1$ will bias the final output to the initial state. However, as Figure 5indicates, such an effect is observed only for extremely small values of $\alpha \in (0, 0.005)$. In addition, there is a large enough range for $\alpha \in (0.005, 0.08)$ where the final output of FastRNN is not biased and is easily learnt by FastRNN.

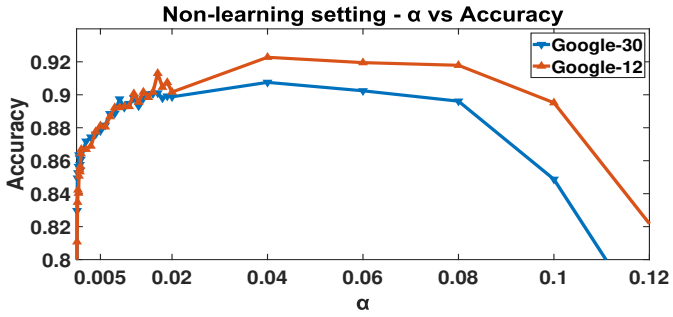

Figure 5: Accuracy vs α in non-learning setting where the parameters of the classifier was learnt and evaluated for a range of fixed α values (using 99 timesteps).

α and β of FastRNN: α and β are the trainable weights of the residual connection in FastRNN. Section 3.1.1 shows that FastRNN has provably stable training for the setting of $\alpha/\beta = O(1/T)$. Table 7 shows the learnt values of α and β for various timesteps (T) across 3 datasets.

Table 7: Scaling of α and β vs Timesteps for FastRNN with $\tanh$ non-linearity: With α set as a trainable parameter, it scales as $O(1/T)$ with the number of timesteps as suggested by Theorem 3.1.

Google-12			HAR-2			MNIST-10		
Timesteps	α	β	Timesteps	α	β	Timesteps	α	β
99	0.0654	0.9531	128	0.0643	0.9652	112	0.0617	0.9447
33	0.2042	0.8898	64	0.1170	0.9505	56	0.1193	0.9266
11	0.5319	0.7885	32	0.1641	0.9606	28	0.2338	0.8746
9	0.5996	0.7926	16	0.2505	0.9718	14	0.3850	0.8251
3	0.6878	0.8246	8	0.3618	0.9678	7	0.5587	0.8935

D Compression Components of FastGRNN

The Compression aspect of FastGRNN has 3 major components: 1) Low-rank parameterization (**L**) 2) Sparsity (**S**) and 3) Byte Quantization (**Q**). The general trend observed across dataset is that low-rank parameterization increase classification accuracies while the sparsity and quantization help reduced the model sizes by 2x and 4x respectively across datasets.

Tables 8, 9 and 10 show the trend when each of the component is gradually removed from FastGRNN to get to FastGRNN-LSQ. Note that the hyperparameters have been re-tuned along with the relevant constraints to obtain each model in the table. Figure 6 shows the effect of each of LSQ components for two Google datasets.

E Hyperparameters of FastGRNN for reproducibility:

Table 11 lists the hyperparameters which were used to run the experiments with a random-seed of 42 on a P40 GPU card with CUDA 9.0 and CuDNN 7.1. One can use the Piece-wise linear approximations of $\tanh$ or sigmoid if they wish to quantize the weights.

F Timing Experiments on more IoT boards

Table 12 summarizes the timing results on the Raspberry Pi which has a more powerful processor as compared with Arduino Due. Note that the Raspberry Pi has special instructions for floating point

Table 8: Components of Compression

Dataset	FastGRNN		FastGRNN-Q		FastGRNN-SQ		FastGRNN-LSQ	
	Accuracy (%)	Model Size (KB)	Accuracy (%)	Model Size (KB)	Accuracy (%)	Model Size (KB)	Accuracy (%)	Model Size (KB)
Google-12	92.10	5.50	92.60	22	93.76	41	93.18	57
Google-30	90.78	6.25	91.18	25	91.99	38	92.03	45
HAR-2	95.59	3.00	96.37	17	96.81	28	95.38	29
DSA-19	83.73	3.25	83.93	13	85.67	22	85.00	208
Yelp-5	59.43	8.00	59.61	30	60.52	130	59.51	130
Pixel-MNIST-10	98.20	6.00	98.58	25	98.72	37	98.72	71

Table 9: Components of Compression for Wakeword-2

Dataset	FastGRNN		FastGRNN-Q		FastGRNN-SQ		FastGRNN-LSQ	
	F1 Score	Model Size (KB)	F1 Score	Model Size (KB)	F1 Score	Model Size (KB)	F1 Score	Model Size (KB)
Wakeword-2	97.83	1	98.07	4	98.27	8	98.19	8

Table 10: Components of Compression for PTB

Dataset	FastGRNN		FastGRNN-Q		FastGRNN-SQ		FastGRNN-LSQ	
	Test Perplexity	Model Size (KB)	Test Perplexity	Model Size (KB)	Test Perplexity	Model Size (KB)	Test Perplexity	Model Size (KB)
PTB-10000	116.11	38.5	115.71	154	115.23	384	115.92	513

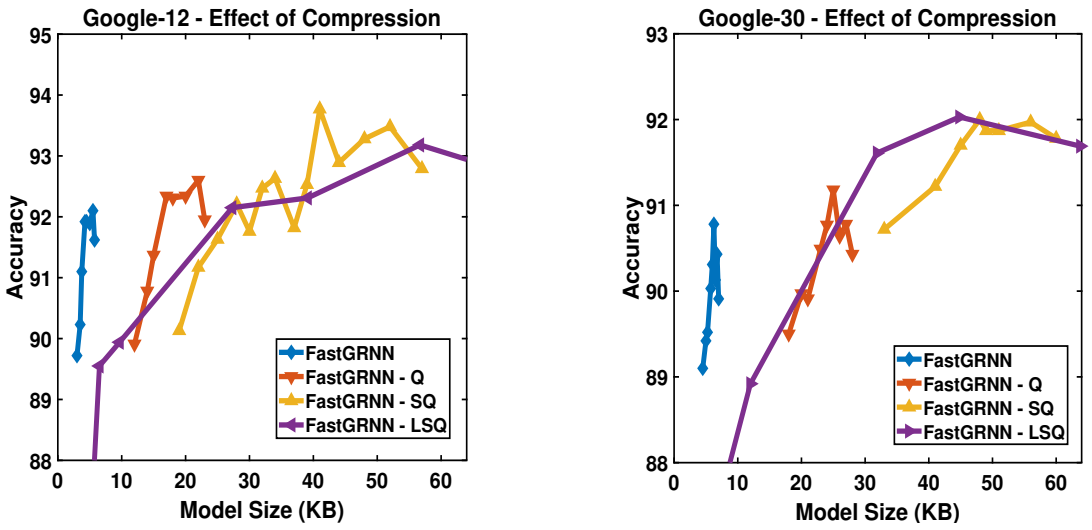

(a) (b)

Figure 6: Figures (a) and (b) show the effect of LSQ components over the model size range of 0-64KB.

arithmetic and hence quantization doesn't provide any benefit with respect to compute in this case, apart from bringing down the model size considerably.

G Vectorized FastRNN

As a natural extension of FastRNN, this paper also benchmarked FastRNN-vector wherein the scalar α in FastRNN was extended to a vector and β was substituted with $\zeta(1-\alpha)+\nu$ with ζ and ν are trainable scalars in $[0, 1]$. Tables 13, 14 and 15 summarize the results for FastRNN-vector and a direct comparison shows that the gating enable FastGRNN is more accurate than FastRNN-vector. FastRNN-vector used $\tanh$ as the non-linearity in most cases except for a few (indicated by $^+$) where ReLU gave slightly better results.

Table 11: Hyperparameters for reproducibility - FastGRNN-Q

Dataset	Hidden Units	r_w	r_u	s_w	s_u	Nonlinearity	Optimizer
Google-12	100	16	25	0.30	0.30	sigmoid	Momentum
Google-30	100	16	35	0.20	0.20	tanh	Momentum
Wakeword-2	32	10	15	0.20	0.30	tanh	Momentum
Yelp-5	128	16	32	0.30	0.30	sigmoid	Adam
HAR-2	80	5	40	0.20	0.30	tanh	Momentum
DSA-19	64	16	20	0.15	0.05	sigmoid	Adam
Pixel-MNIST-10	128	1	30	1.00	0.30	sigmoid	Adam
PTB-10000	256	64	64	0.30	0.30	sigmoid	Adam

Table 12: Prediction Time on Raspberry Pi 3 (ms)

Method	Google-12	HAR-2	Wakeword-2
FastGRNN	7.7	1.8	2.5
RNN	15.7	2.9	3.6
UGRNN	29.7	5.6	9.5
SpectralRNN	123.2	391.0	17.2

Table 13: FastRNN Vector - 1

Dataset	Accuracy (%)	Model Size (KB)	Train Time (hr)
Google-12	92.98$^+$	57	0.71
Google-30	91.68$^+$	64	1.63
HAR-2	95.24$^+$	19	0.06
DSA-19	83.24	322	0.04
Yelp-5	57.19	130	3.73
Pixel-MNIST-10	97.27	44	13.75

Table 14: FastRNN Vector - 2

Dataset	F1 Score	Model Size (KB)	Train Time (hr)
Wakeword-2	97.82	8	0.86

Table 15: FastRNN Vector - 3

Dataset	Test Perplexity	Train Perplexity	Model Size (KB)	Train Time (min)
PTB-300	126.84	98.29	513	11.7

H Effects of Regularization for Language Modeling Tasks

This section studies the effect of various regularizations for Language Modeling tasks with the PTB dataset. [36] achieved state-of-the-art performance on the PTB dataset using a variety of different regularizations and this sections combines those techniqeus with FastGRNN and FastGRNN-LSQ. Table 16 summarizes the train and test perplexity of FastGRNN. The addition of an extra layer leads to a reduction of 10 points on the test perplexity score as compared to a single layer architecture of FastGRNN. Other regularizations like weight decay and weight dropping also lead to gains of upto 8 points in test perplexity as compared to the baseline FastGRNN architecture, exhibiting that such regularization techniques can be combined with the proposed architectures to obtain better dataset specific performance, especially on the language modelling tasks of the PTB dataset.

The experiments carried out in this paper on the PTB dataset use a sequence length of 300 as compared to those used in [38, 53, 21, 35, 36] which are generally in the range of 35-70. While standard recurrent architectures are known to work with such short sequence lengths, they typically exhibit unstable behavior in the regime where the sequence lengths are longer. These experiments exhibit the stability properties of FastGRNN (with 256 hidden units) in this regime of long sequence lengths with limited compute and memory resources.

Table 16: Language Modeling on PTB - Effect of regularization on FastGRNN

Method	Hidden Units	Test Perplexity	Train Perplexity
1-layer	256	116.11	81.31
2-layer	256	106.23	69.37
1-layer + Weight decay	256	111.57	76.89
1-layer + Weight-dropping	256	108.56	72.46
1-layer + AR/TAR	256	112.78	78.79